Masters Theses

Student Theses and Dissertations

Spring 2017

High speed serial link design with multi-level signaling and characteristic impedance extraction from a transmission line with meshed ground planes

Jiayi He

Follow this and additional works at: https://scholarsmine.mst.edu/masters_theses

Part of the Electrical and Computer Engineering Commons

Department:

Recommended Citation

He, Jiayi, "High speed serial link design with multi-level signaling and characteristic impedance extraction from a transmission line with meshed ground planes" (2017). *Masters Theses*. 7646.
https://scholarsmine.mst.edu/masters_theses/7646

HIGH SPEED SERIAL LINK DESIGN WITH MULTI-LEVEL SIGNALING AND

CHARACTERISTIC IMPEDANCE EXTRACTION FROM A TRANSMISSION LINE

WITH MESHED GROUND PLANES

by

JIAYI HE

A THESIS

Presented to the Faculty of the Graduate School of the

MISSOURI UNIVERSITY OF SCIENCE AND TECHNOLOGY

In Partial Fulfillment of the Requirements for the Degree

MASTER OF SCIENCE IN ELECTRIC ENGINEERING

2017

Approved by

Dr. Jun Fan, Advisor
Dr. Nana Dikhaminjia, Co-advisor
Dr. James Drewniak
Dr. Mikheil Tsiklauri

ABSTRACT

Channel bandwidth and manufacturing process have become two limitations in today's high speed designs. In order to overcome the channel bandwidth limitation, multilevel signaling is seen as one of the ways to achieve higher data rates. Using multilevel signaling as the coding scheme will impose new challenges in high speed serial link design. Due to manufacturing limitations, only transmission lines with meshed ground planes are allowed in some applications. Meshed power and ground planes have been widely used in today's flexible PCB designs to satisfy repeatability installation and reliability requirements.

In Section 1, high speed serial link design with PAM4 signaling is investigated. Specifics of DFE and FFE equalizers for PAM4 are discussed. Tests on channels with different properties are done to reveal the advantages and drawbacks of PAM4 compared to NRZ.

In Section 2, an equivalent transmission line model is used to extract the effective characteristic impedance of the transmission lines with meshed ground planes. The results are confirmed with full-wave simulations. Then by using DoE method, the characteristic impedance can be predicted when the geometry is in a given range.

ACKNOWLEDGMENTS

I would like to express my great gratitude to my advisor, Dr. Jun Fan, for his guidance, encouragement, and trust throughout my master study. I learned a lot from him not only at the technical side, but also the non-technical side. He helped me gain a big picture of how to deal with research work, the people around, and also family. I feel fortunate to work with him and be his student.

I would also like to thank my co-advisor, Dr. Nana Dikhaminjia, who guided me how to manage a project. I learned a lot from her too. I would like to thank Dr. James Drewniak and Dr. Mikheil Tsiklauri for their advice and help on my research work.

I also feel grateful to Xiang Fang, Feng Zhang, Qiaolei Huang, Siqi Bai, Chunyu Wu, Yansheng Wang, Guangyao Shen. Every one of them helped me a lot in my research and life in Rolla. Also my thanks go to all of the other faculty members and my fellow lab mates in the EMC group of Missouri S&T. I am happy to work with you.

Finally, my sincere appreciation goes to my mother. I dedicate this thesis to her.

TABLE OF CONTENTS

LIST OF ILLUSTRATIONS

LIST OF TABLES

1. HIGH SPEED SERIAL LINK DESIGN USING MULTI-LEVEL SIGNALING

1.1. INTRODUCTION

Multi-level signaling is widely discussed in recent years as an alternative coding scheme to binary modulation NRZ (Non Return to Zero) signaling to overcome the bandwidth limitations of the channel and respond to the increasing demand for higher data rates. Now most attention is paid to PAM4 (Pulse Amplitude Modulation). The standard amendment 802.3bj "Physical Layer Specifications and Management Parameters for 100Gb/s Operation over Backplanes and Copper Cables" defines two different approaches for 100Gb/s backplane – using PAM4 and NRZ coding[1][2]. PAM4 is also topic of active discussion of the Study Group on the upcoming standard 802.3bs for Development of the IEEE P802.3bs 400 Gigabit Ethernet (GbE) project that considers 100Gbps over each of 4 lanes or 50Gbps over each of 8 lanes[3].

PAM4 encodes two NRZ bits in one symbol. Figure 1.1 shows an example of converting binary signal to PAM4 signal using gray-coding. Since 4 levels impose new challenges and constraints on the usage of this modulation type, it is important to reveal the similarities and differences in link-path analysis for both signaling type, as well as to provide comparison analysis with NRZ for different types of serial links and backplanes. The equalizers also play an important role with PAM4 encoding, thus the methodology of equalizations also needs to be defined for PAM4 signaling. The PAM4 methodology will also open a new door for other higher order modulation schemes, such as PAM8, PAM16, etc.
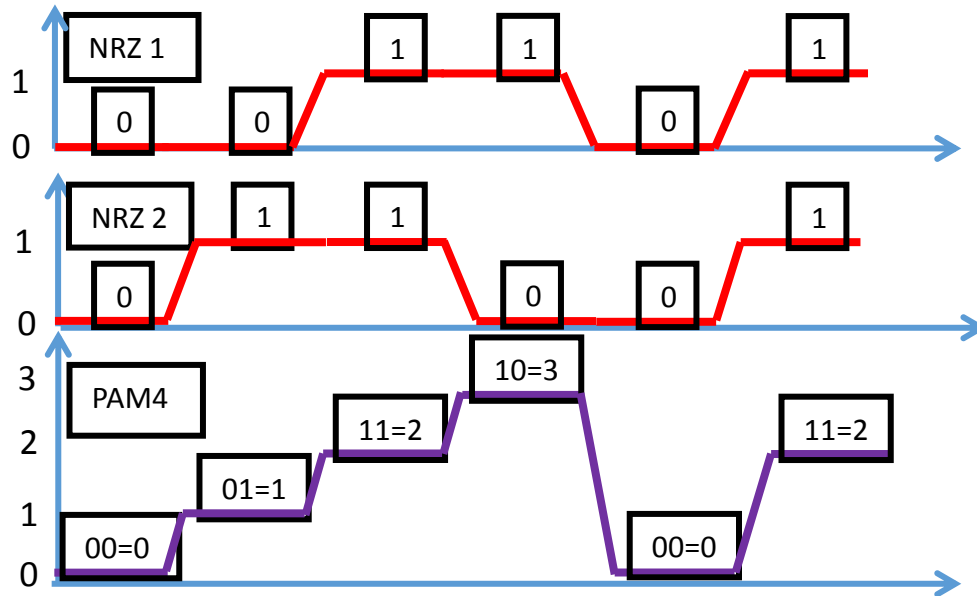
Figure 1.1. Gray-coding of NRZ signal to PAM4 signal

1.2. ADVANTAGES AND CHALLENGES OF PAM4 SIGNALING

PAM4 allows achieving the same data rate using half of the bandwidth compared to NRZ. Considering that the channel bandwidth has become one of the main limitations in today's high speed system designs, using PAM4 encoding scheme can be a good solution to overcome it. Since the symbol rate with PAM4 is half that of NRZ, the signal suffers less from channel loss as shown in Figure 1.2. As crosstalk is often of high-pass feature, the crosstalk to insertion loss ratio may be larger at half of the frequency bandwidth (Nyquist frequency for NRZ) than one fourth of the frequency bandwidth (Nyquist frequency for PAM4)[4]. Also the unit interval or symbol length for PAM4 will be twice the length of an NRZ symbol, so PAM4 tends to have a larger eye width. The advantages of PAM4 at channel loss make it possible to achieve high-speed systems with cheap and lossy materials.
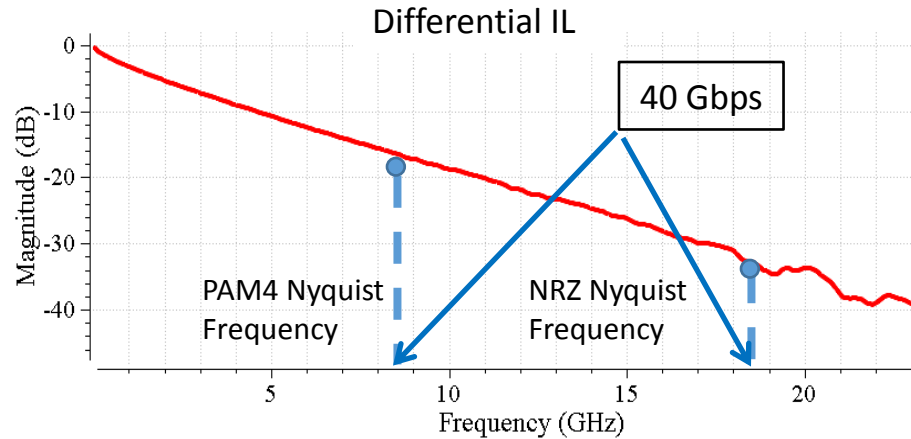
Figure 1.2. Insertion loss comparison between PAM4 and NRZ

The 4-level for PAM4 brings some challenges. First of all, additional voltage levels with PAM4 reduce level spacing by a factor of 3 (9.5 dB), as it has three eyes instead on one eye of NRZ. It also means that the receiver must have three slicers – one slicer for each eye. Definition of proper slicers are important for PAM4 as the DFE equalizer, bathtub and BER calculation will depend on the slicers[6][7]. Upper and lower slicers for PAM4 can be defined as intersection of transitions (2-3; 3-2) and (0-1; 1-0), respectively as shown in Figure 1.3.
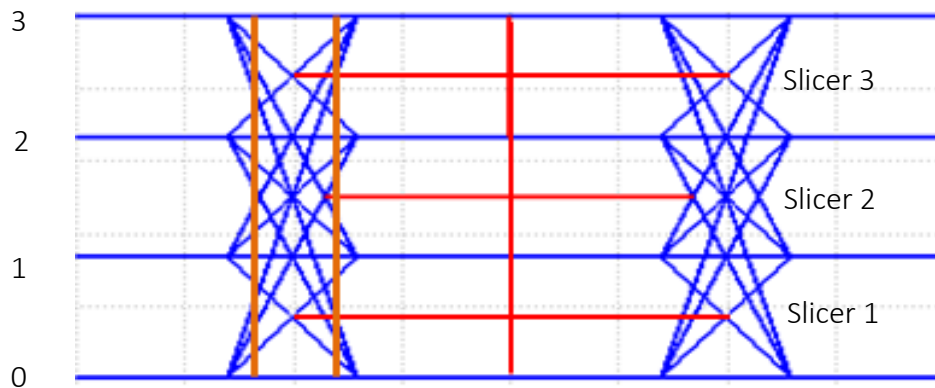
Figure 1.3. PAM4 slicers

Additional challenge is presented by 16 transitions of PAM4 as opposed to 4 transitions of NRZ. These 16 transitions will cause inherent transition jitter in PAM4 signal. From Figure 1.4, it can be shown that the eye width of the upper eye or lower eye

is $2\text{UI}-2/3\text{t\_rise}$, less than 2UI even before the channel, where UI is the unit interval for NRZ. The inherent transition jitter is one third of the rise time. The upper eyes and lower eyes are also not symmetrical regarding horizontal slicers even in ideal conditions, which makes it more difficult to translate eye diagram results correctly.

W – Eye width   Transition Jitter = 1/3 t_rise
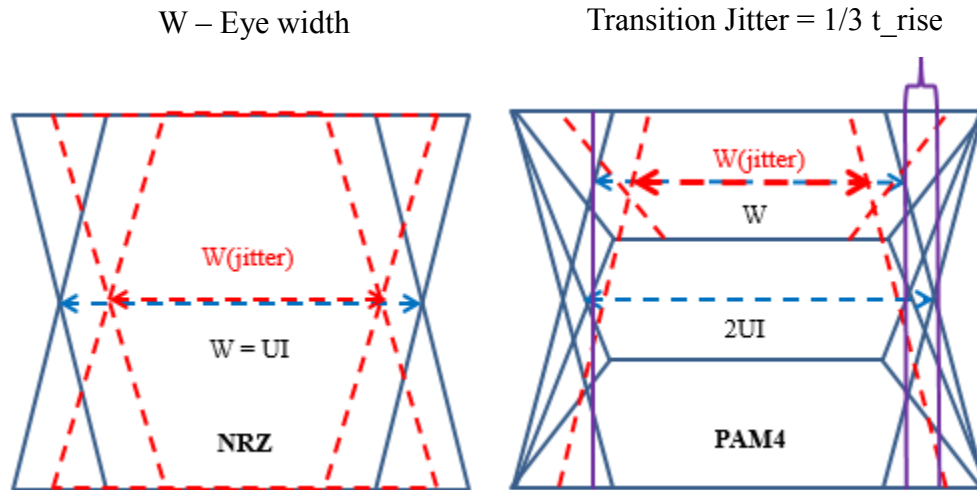
Figure 1.4. PAM4 transition jitter

Assume the total transmission jitter of UI in percentage is p, so the NRZ eye width at transmission side is equal to $(1\text{-}2\text{p})\text{UI}$. The PAM4 upper eye width with the same amount of jitter is $(1\text{-}2\text{p})\times2\text{UI}-2/3\text{t\_rise}$. If NRZ eye width and PAM4 eye width are the same, then $\text{p}=1/2\text{-t\_rise}/3/\text{UI}$. Assume the rise time is 20 percent of the unit interval of PAM4, which means $\text{t\_rise}/2\text{UI}=0.2$, therefore $\text{p}=0.36$. So if 36% of NRZ UI is considered, then the eye width before the channel for PAM4 and NRZ will be the same without taking jitter amplification into account.

1.3. EQUALIZATION SPECIFICS FOR PAM4 SIGNALING

The equalizers also play an important role with PAM4 encoding. FFE and DFE are two common equalizers that are widely used in serial link systems.

1.3.1. FFE for PAM4. FFE is the abbreviation for feed-forward equalizer, which is a finite impulse response (FIR) filter as shown in Figure 1.5. The output of the equalizer, y(k), is expressed as the discrete convolution of the input signal, x(k), with the equalizer tap coefficients, c_n, :

$$y(k) = \sum_{n=-N}^{N} x(k-n) \times c_n \tag{1}$$
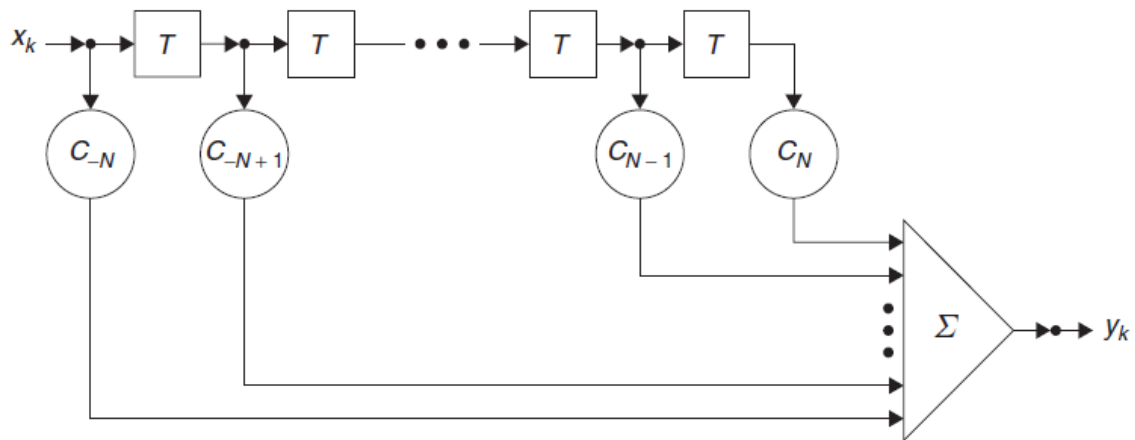
Figure 1.5. Feed-forward equalizer

FFE for PAM4 in general is the same as for NRZ. But the overshooting affects PAM4 more, so the main cursor of FFE for PAM4 cannot be taken as low as for NRZ. This effect can be seen easily at the transmitter side. By applying a two-tap de-emphasis at the transmitter, the highest level 0 is $1-2c_0$ and the lowest level 1 is $2c_0-1$. So the level 0 and level 1 start to mix when the main cursor, c_0, is less than 0.5 for NRZ. But for PAM4 levels, they start to intersect when the FFE main cursor is less than 0.75. For example, the

first-to-third levels are equalized to $-c_1 + c_0 / 3$ and fourth-to-fourth levels are equalized to

$c_1 + c_0$. Since $c_1 = c_0 - 1$, if $-c_1 + c_0/3 > c_1 + c_0$, then c_0 is less than 0.75 as illustrated in

Figure 1.6. Obviously, the PAM4 levels will not mix at the receiver due to channel loss

when the main cursor is 0.75 and the more lossy is the channel, the lower the FFE main

cursor can go. But in the overall, FFE of multi-level signal has always more restriction of

the main cursor, comparing to NRZ, to avoid level intersection.
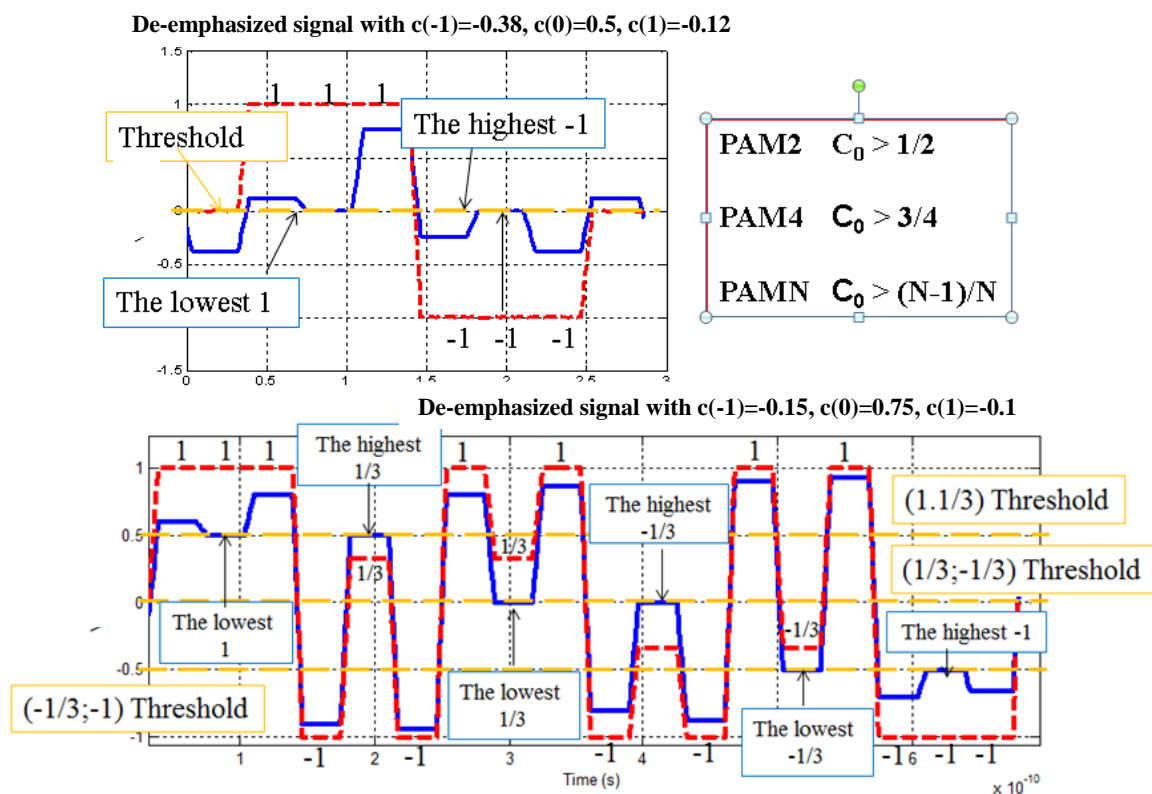
Figure 1.6. Level mixing in NRZ and PAM4

For example, the 3-tap FFE with least mean square optimization is applied at the

data rate that the difference between insertion losses at Nyquist Frequencies for both

signals is 9.5dB. Obtained coefficients are (-0.1, 0.57, -0.33) for NRZ and (-0.05, 0.72, -

0.23) for PAM4. If the coefficients of NRZ are used for PAM4, all 3 eyes decrease as shown in Figure 1.7 because of overshooting and mixing of levels.
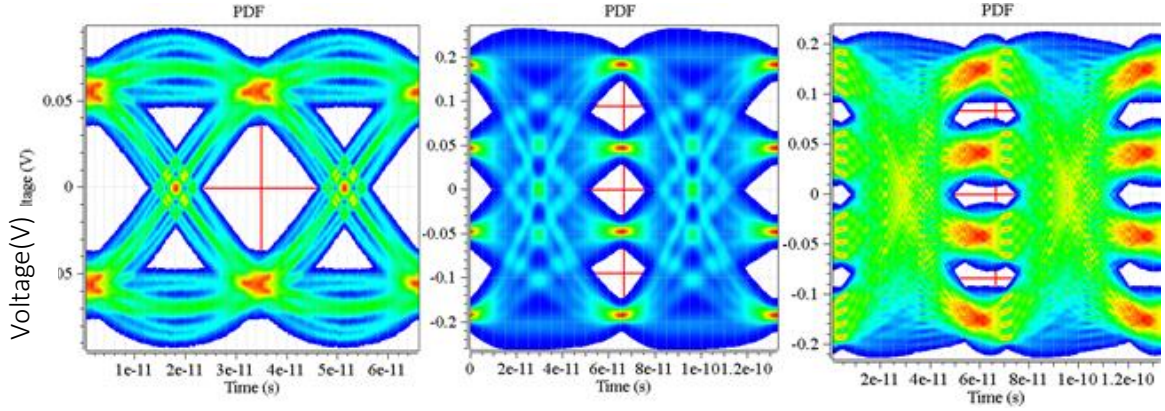
Figure 1.7. Level-mixing effects in PAM4

1.3.2. DFE for PAM4. The decision feedback equalizer (DFE) is a non-linear filter that makes use of previous decisions to estimate and subtract inter-symbol interference (ISI) from the input stream. The slicer makes a symbol decision when a signal comes and the results are fed back to the slicer input to cancel ISI. The formula for an ideal DFE is:

$$V_k^{DFE} = V_k - d_1 f\left(V_{k-UI}^{DFE}\right) - d_2 f\left(V_{k-2UI}^{DFE}\right) - \ldots - d_n f\left(V_{k-nUI}^{DFE}\right) \qquad (2)$$

Where V_k^{DFE} is the output of the decision feedback equalizer, V_k is the input stream and $f(x)$ is the decision making function at the slicer. For PAM4 signaling, $f(x)$ is calculated as follows:

$$
\begin{aligned}
&f(x)=1 \ \ if \ \ slicer_3 \le x; \\
&f(x)=1/3 \ if \ \ slicer_2 \le x \le slicer_3, \\
&f(x)=-1/3 \ if \ \ slicer_1 \le x \le slicer_2; \\
&f(x)=-1 \ if \ \ x \le slicer_1
\end{aligned}
\qquad (3)
$$

In reality, DFE is often used together with FFE or CTLE. So the FFE and DFE combined optimization becomes another challenge. If the optimized tap values for FFE only are used, the results are usually worse after DFE. An example is shown in Figure 1.8 and Figure 1.9.
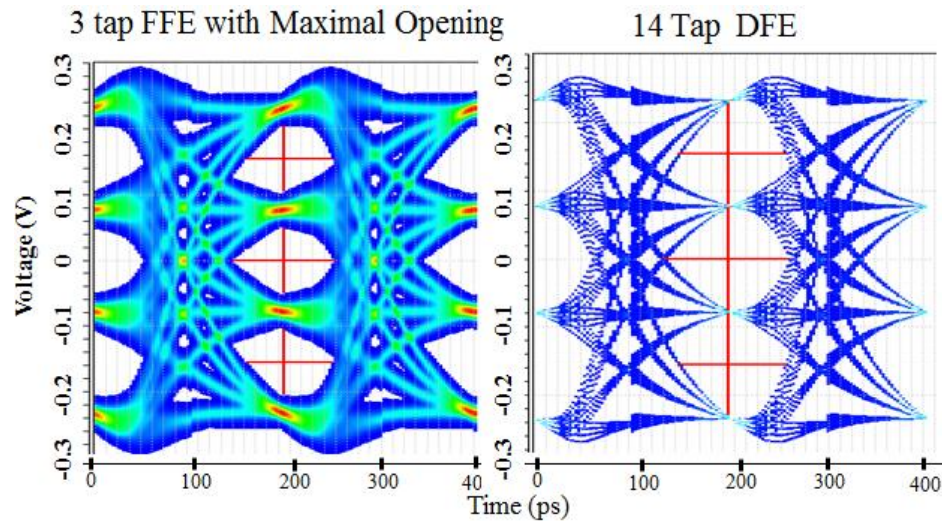
Figure 1.8. Eye opening with 0.77 FFE main tap
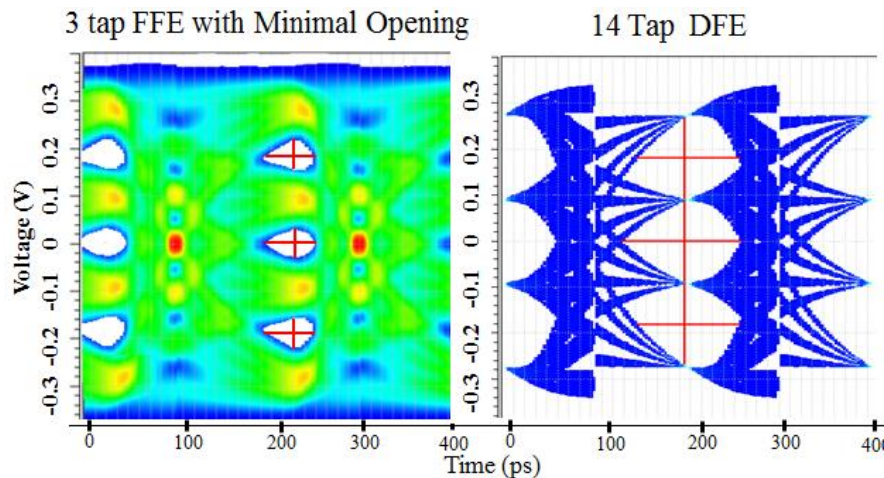
Figure 1.9. Eye opening with 0.92 FFE main tap

The FFE coefficients are chosen by least-mean-square optimization and the eye height after FFE is 101mV in Figure 1.8. Then after an optimized 14-tap DFE, the final

eye height is 151mV. In Figure 1.9 only 55mV eye height is obtained after FFE, but finally

180mV eye height is achieved after DFE, which is about 20% more than the previous case.

The main reason of this effect is that the signal level is decreased when the main

cursor of the FFE coefficients goes lower. The FFE main cursor value is 0.77 in the first

case, while 0.92 in the second case. The DFE in both cases can remove the ISI efficiently

but the signal level in the first case is lower. So the FFE and DFE combined optimization

is another challenge for PAM4.

1.4. COMPARISON TESTS BETWEEN PAM4 AND NRZ

The transient simulation for PAM4 signaling is integrated into FEMAS, the internal

channel analysis tool. Comparison tests are carried out using this tool.

1.4.1. Test Channel Topology and Simulation Methodology. The tests are

done on 12-port S-parameters as shown in Figure 1.10.
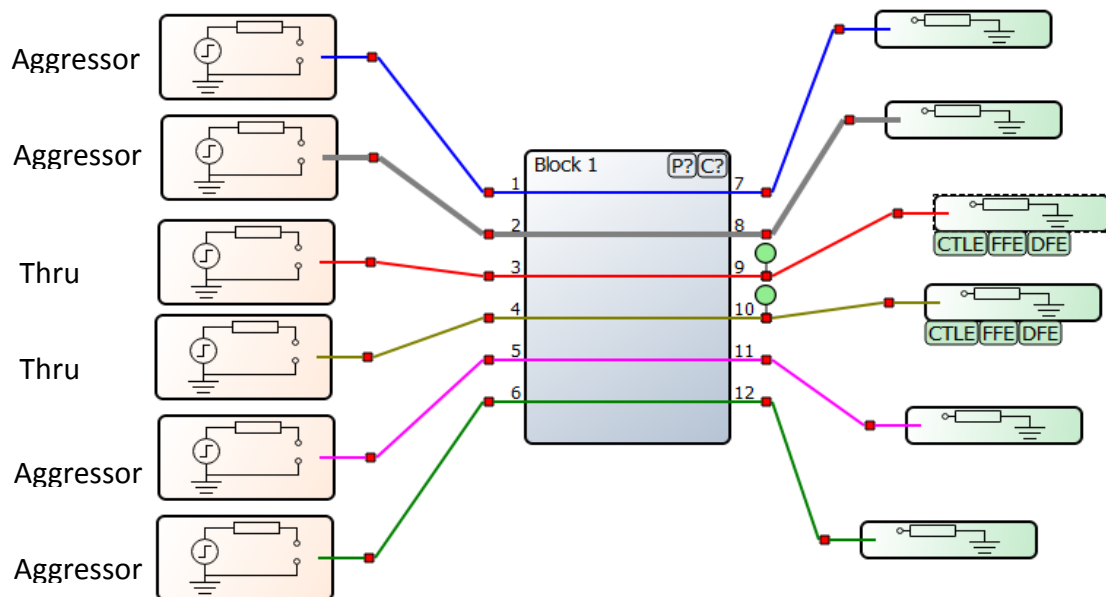
Figure 1.10. Simulation Schematic in FEMAS

For NRZ, pseudo random bit sequence (PRBS14) was used and since PAM4 bit length is twice the length of NRZ, pseudo random quaternary sequence (PRQS7) is used. FFE, CTLE and DFE are used as equalizers. For finding best tap coefficients, least-square optimization methods are used. Optimization methods for PAM4 equalizers are using the same approach as for NRZ, but are adjusted for three slicers of PAM4. For comparison purposes, the same number of tap coefficients was used for the same speed NRZ and PAM4. Simulation includes one differential 'Thru' and two differential aggressors. On transmitter side, random jitter with 5% of UI and periodic jitter with 10% of UI amplitude and 10 MHz frequency are injected. Rise-fall time is taken 20% of UI for each channel. Source and termination impedances are matched. Figure 1.11 shows the channel structure.
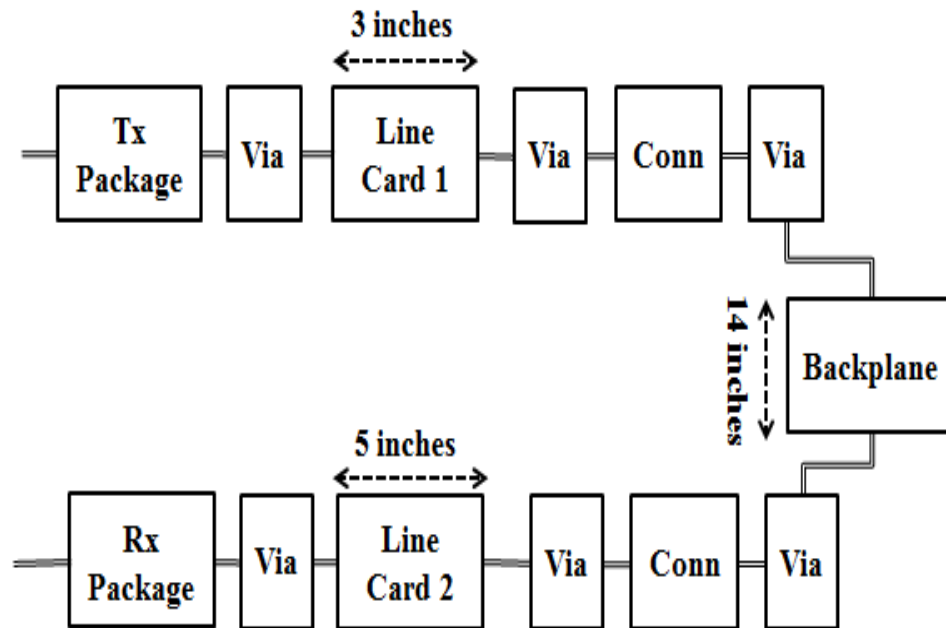
Figure 1.11. The structure of the end to end channel topology

The block structure given in the above figure is an end to end channel topology with 2 daughter cards connected together using a backplane with two high speed connectors

in the path. The overall trace length is 22 inches with 3 inches on line card 1, 14 inches on backplane and 5 inches on line card 2.

Simulations have been performed for the following data rates: 10 Gbps, 16 Gbps, 20 Gbps, 25 Gbps, 28 Gbps, 32 Gbps, 40 Gbps, 50 Gbps and 56 Gbps. The equalizers used for each data rate are given in Table 1.1:

Table 1.1. Equalizer setting in the tests

Data rate	FFE	DFE	CTLE
10 Gbps	5-tap	No	No
16 Gbps	5-tap	5-tap	No
20 Gbps	5-tap	5-tap	No
25 Gbps	5-tap	6-tap	No
28 Gbps	5-tap	7-tap	Yes
32 Gbps	5-tap	8-tap	Yes
40 Gbps	5-tap	9-tap	Yes
50 Gbps	5-tap	10-tap	Yes
56 Gbps	5-tap	10-tap	Yes

1.4.2. Results Analysis Methodology. The eye height results and eye width results of both NRZ and PAM4 simulation results are recorded. An example of NRZ eye diagram and PAM4 eye diagram is shown in Figure 1.12 and Figure 1.13.

The PAM4 eye heights are compared to NRZ eye heights. The data rates that PAM4 gives better eye height results are determined and the dB differences in insertion loss at Nyquist frequency are also obtained as shown in Figure 1.14 and Figure 1.15.
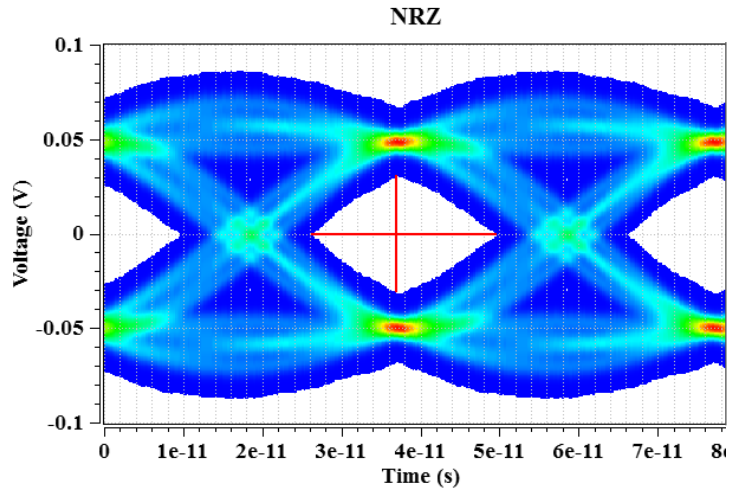
Figure 1.12. NRZ eye diagram in FEMAS
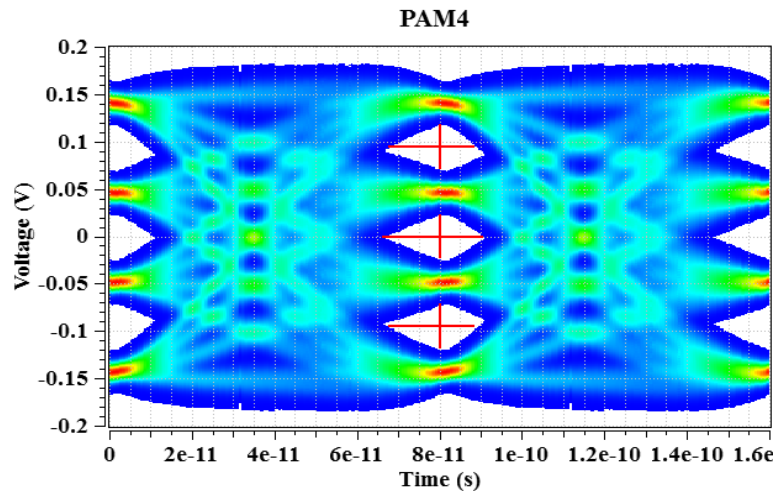
Figure 1.13. PAM4 eye diagram in FEMAS
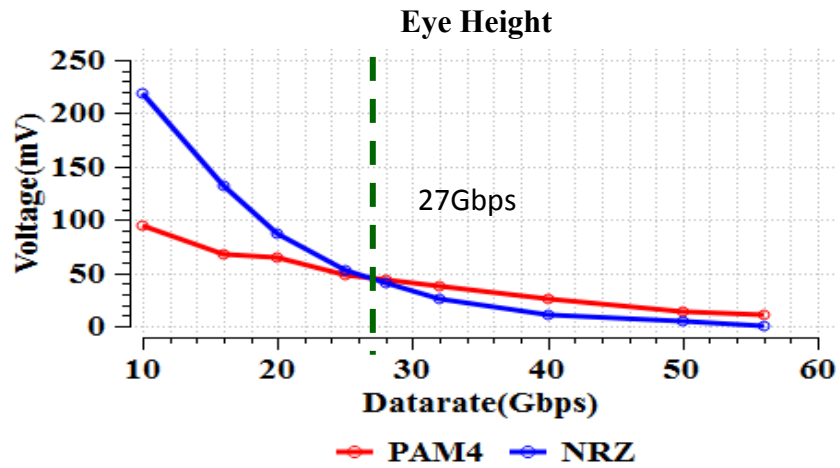
Figure 1.14. Eye heights comparison between NRZ and PAM4

Difference of Insertion Loss for Ny Frequencies at crucial data rate for PAM4 and NRZ
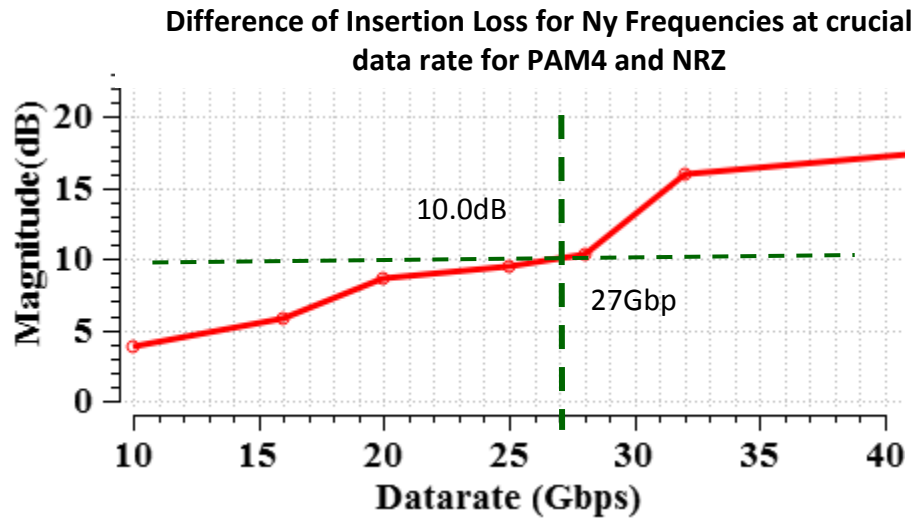
Figure 1.15. Difference of insertion loss for Nyquist frequency at the crucial data rate for PAM4 and NRZ

The PAM4 eye widths are compared to NRZ eye widths as well. As shown in Figure 1.16, PAM4 always gives better eye widths results with these settings in spite of the inherent transient jitter. It is the natural advantage of PAM4 that its UI is twice the UI of NRZ. So most attention is paid to the eye height results in the tests.
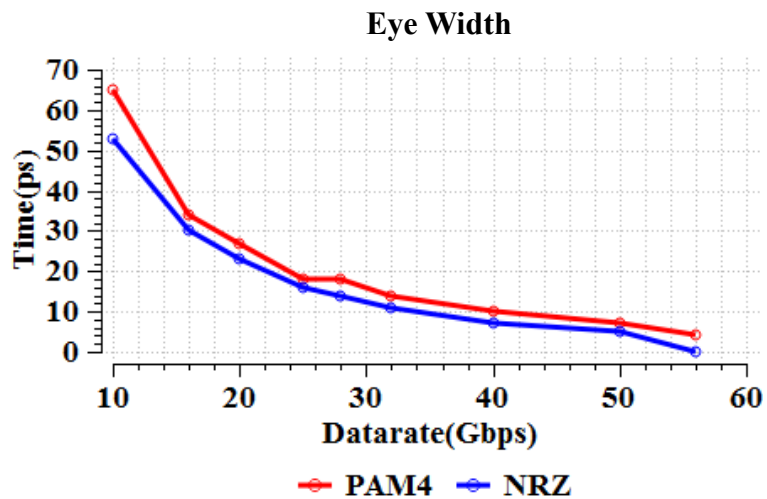
Eye Width

Figure 1.16. Eye widths comparison between PAM4 and NRZ

1.4.3. The Effect of Impedance Mismatch. To investigate the effect of reflection, five files with source and termination impedance ±15% mismatch were tested.

The insertion losses and reflection losses of these five files are shown in Figure 1.17. And Figure 1.18 shows the crucial data rates and dB differences of these five cases. Additional reflection loss affects PAM4 more than NRZ, therefore crucial data rates become higher than the nominal case.

Differential RL

Differential IL

Source and load
Impedance mismatch

H = +15% impedance
L = -15% Impedance

HHLL ── HLHL ── LHLH ── LHLH ── NNNN
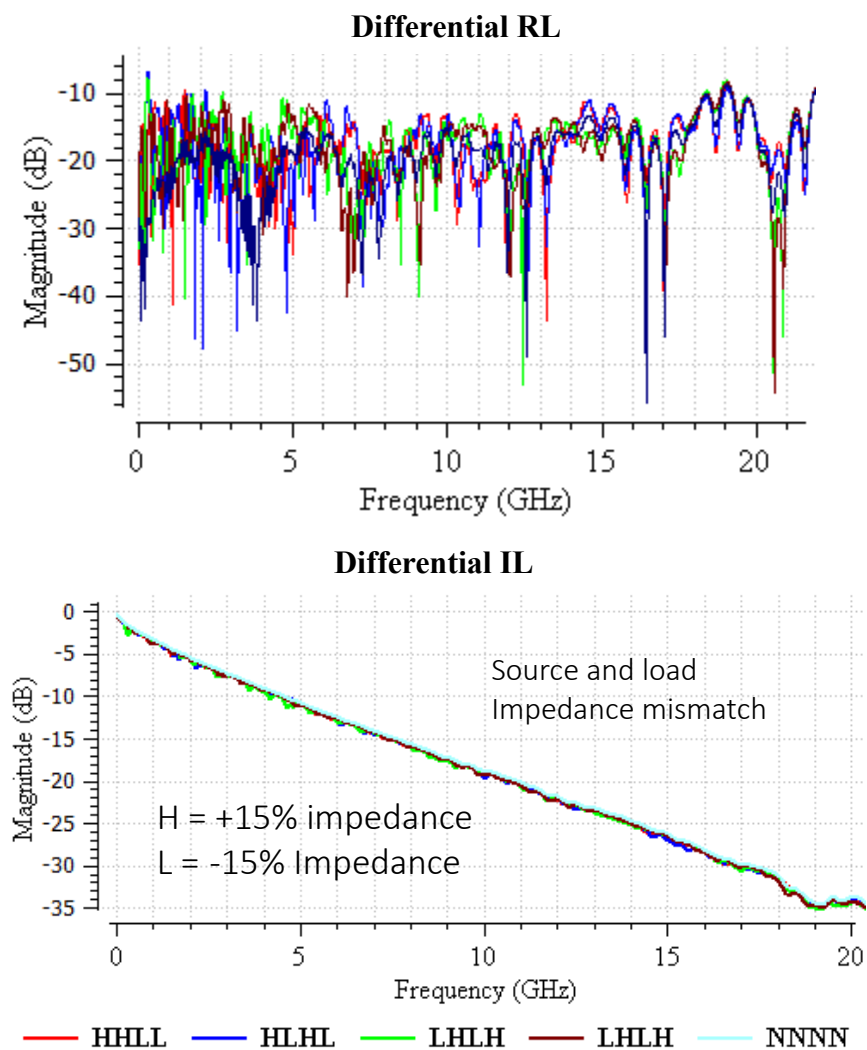
Figure 1.17. Return losses and insertion losses of the files with impedance mismatch
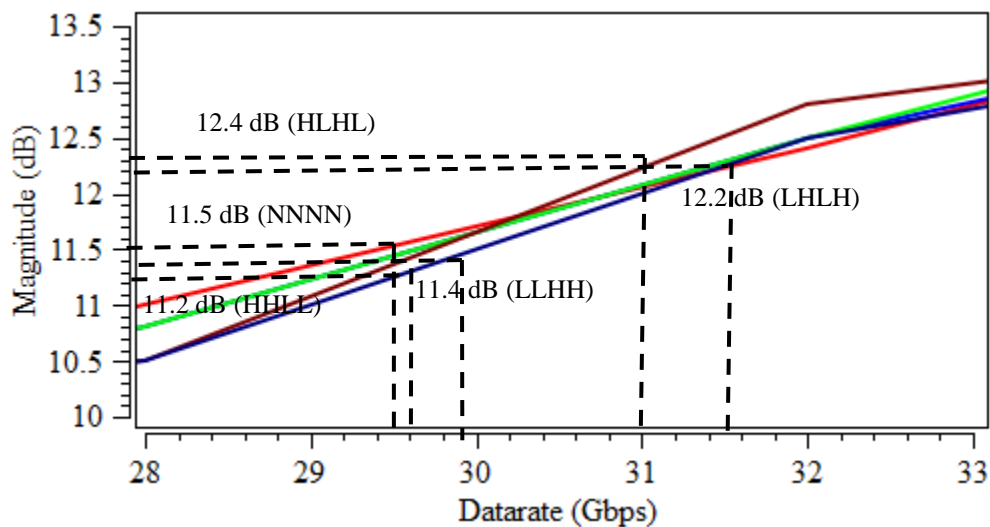
Figure 1.18. The crucial data rates and the corresponding dB differences

1.4.4. Results Comparison with Different Materials. Tests were done on three materials with different loss. The Df values are 0.002, 0.01 and 0.02 respectively. The insertion loss of these three channels are shown in Figure 1.19.
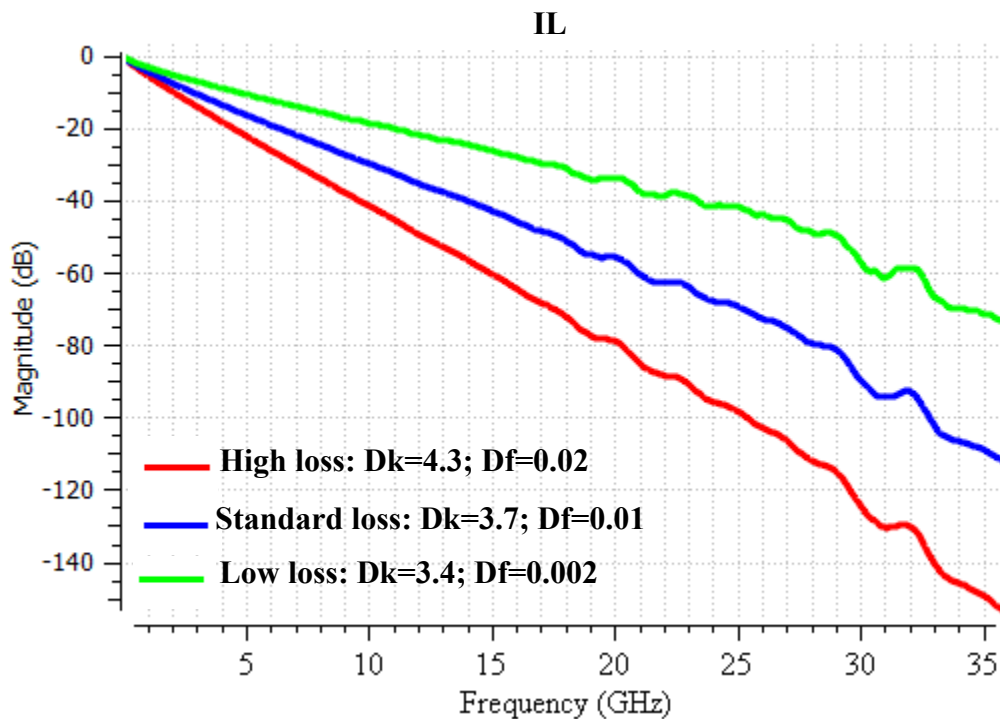
Figure 1.19. The insertion losses of the files with different materials

The eye height comparison results between PAM4 and NRZ for all three materials are shown Figure 1.20 and Table 1.2.

FR4

IS415

MEG6
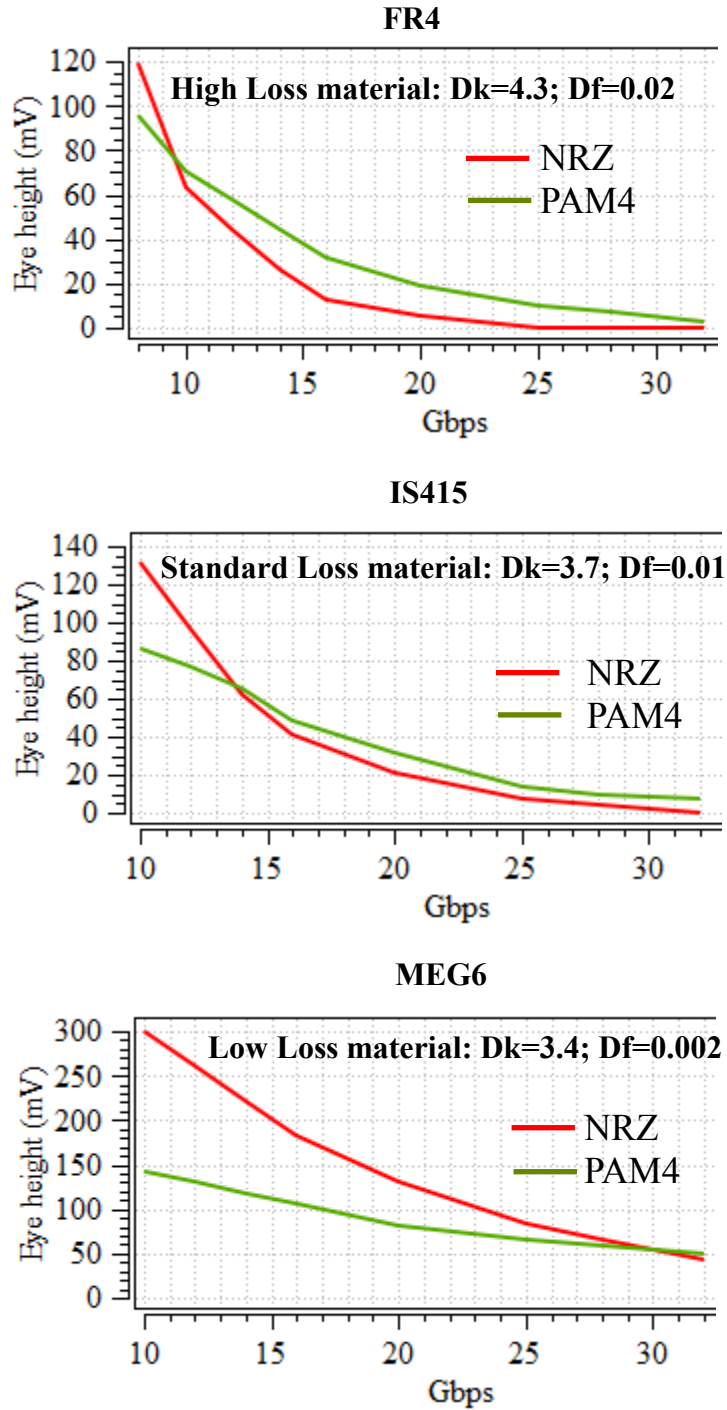
Figure 1.20. Eye height results comparison for the three materials

Table 1.2. Crucial data rates and dB difference for the three materials

	High Loss	Stand. Loss	Low Loss
Data rate (Gbps)	9.5	13.7	29.8
dB Difference	9.7	9.6	11.2

The crucial data rate decreases from 27.5Gbps to 10.9Gbps when the material Df value increases from 0.001 to 0.02. So PAM4 is more efficient with high loss materials and allows more flexibility in material selection.

1.4.5. The Effect of Crosstalk. Tests with far-end crosstalk were done for boards with one victim differential pair and two aggressors. The distance between the victim and the aggressor equals to 3h, 6h, 9h and 12h, where h is the dielectric height as shown in Figure 1.21. The insertion losses and the corresponding crosstalk for all four cases are shown in Figure 1.22. It can been seen that the crosstalk is quite strong in the 3h case but very weak in the 12h case. Results are shown in Figure 1.23 and Figure 1.24.
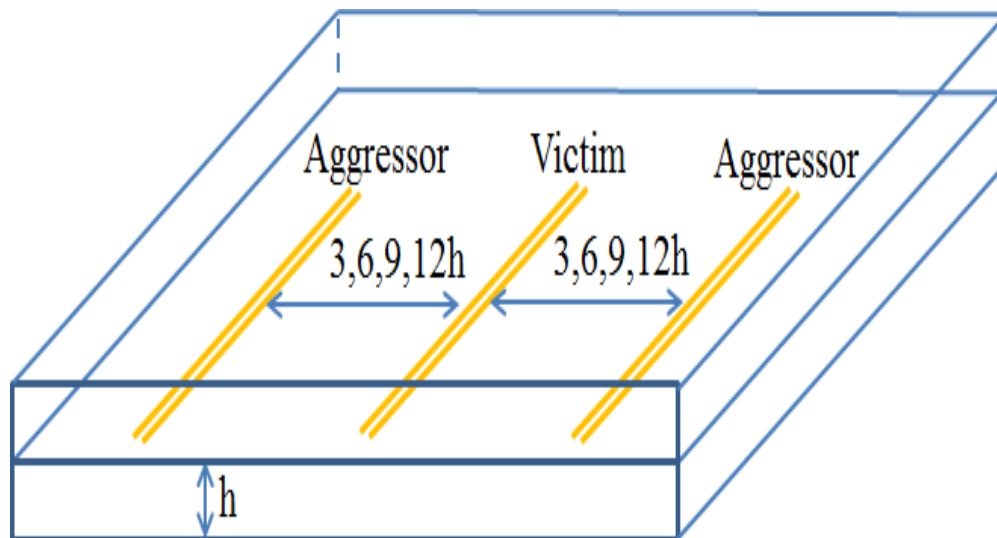
Figure 1.21. The structure of the boards for crosstalk tests
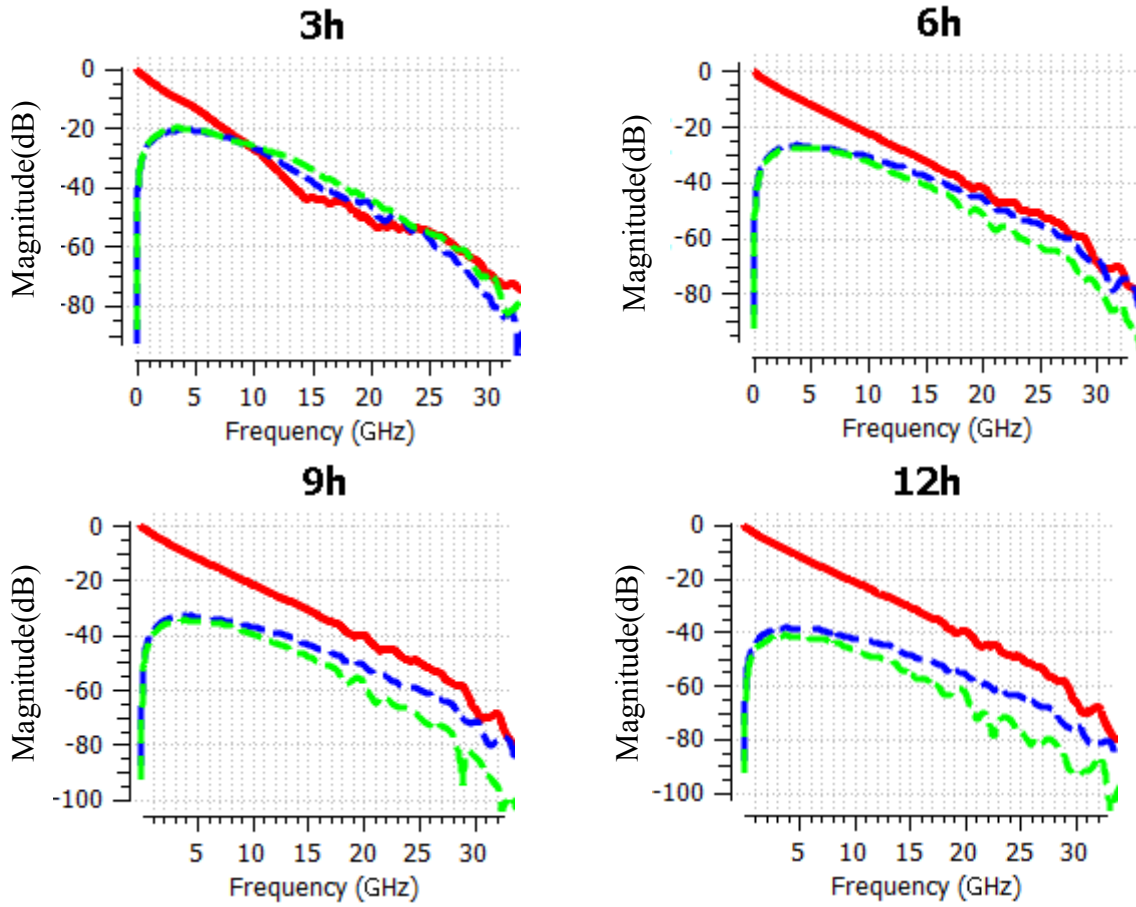
Figure 1.22. Insertion losses of victim and far-end crosstalk of each board
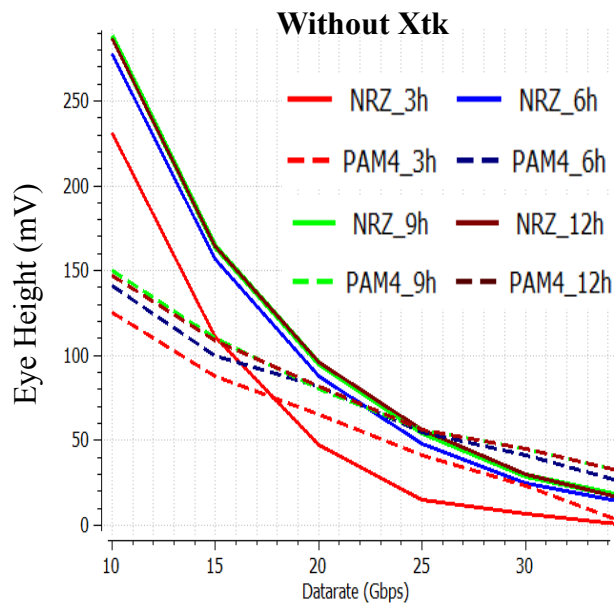
Figure 1.23. Eye height results without crosstalk
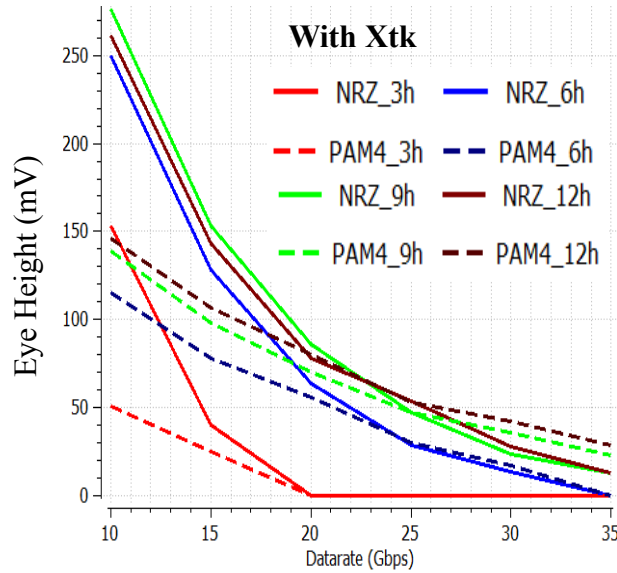
Figure 1.24. Eye height results with crosstalk

The eye height results without crosstalk from 10Gbps to 35Gbps with 5-tap are shown in Figure 1.23. And Figure 1.24 shows the eye height results when crosstalk noise are added. After adding crosstalk, the crucial data rate tends to start later than the cases without crosstalk.

PAM4 and NRZ eye heights closing in percentage caused by crosstalk are also compared in Figure 1.25 and Figure 1.26.
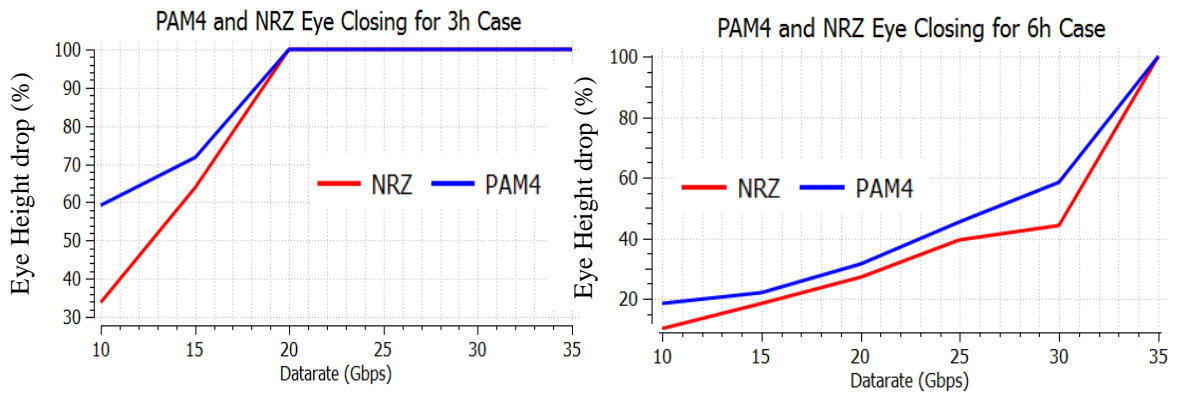
Figure 1.25. Eye heights closing in percentage for 3h and 6h cases
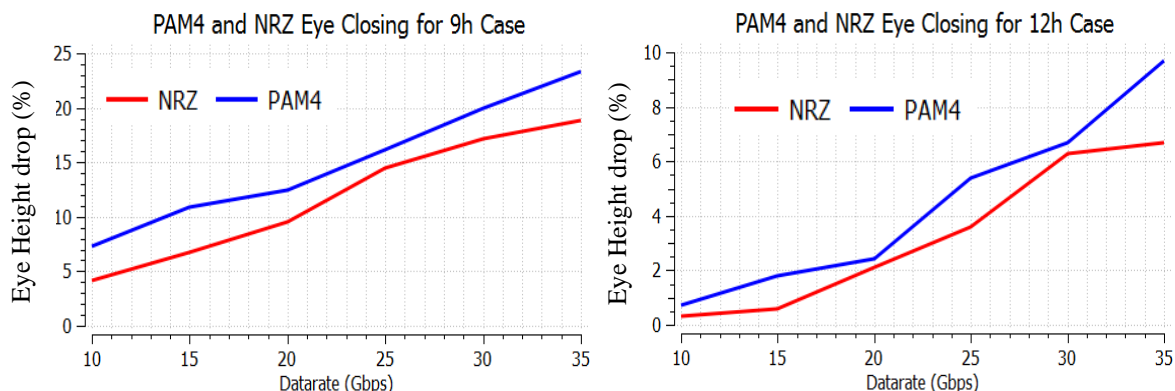
Figure 1.26. Eye heights closing in percentage for 9h and 12h cases

For all 4 cases, the PAM4 eye closing in percentage is larger than NRZ from 10Gbps to 35Gbps. Since crosstalk is additional voltage noise, it is added to 4 different levels for PAM4 but only added to 2 levels for NRZ. As a result, PAM4 eye gets closed more than NRZ, and the crucial data rate starts later due to the crosstalk effect.

1.4.6. Results Comparison with Via Stubs. Test were carried out for the channels with 10, 30, 50, 70, and 90mils via stubs from 10 to 32Gbps. The insertion losses are shown in Figure 1.27.

The eye height and crucial data rate results as shown in Figure 1.28 and Table 1.3 indicate that increasing via stub gives more advantage to PAM4. Since the Nyquist frequency of PAM4 is only one fourth of the frequency bandwidth, it is easier to locate before the resonance caused by via stubs. And the channel frequency response before the fundamental frequency is generally more critical than the harmonics, so PAM4 has more advantage when there is high frequency resonance in the channel. It also means PAM4 has more flexibility in real design, as NRZ requires very short via stubs in manufacturing while PAM4 doesn't.

Differential IL
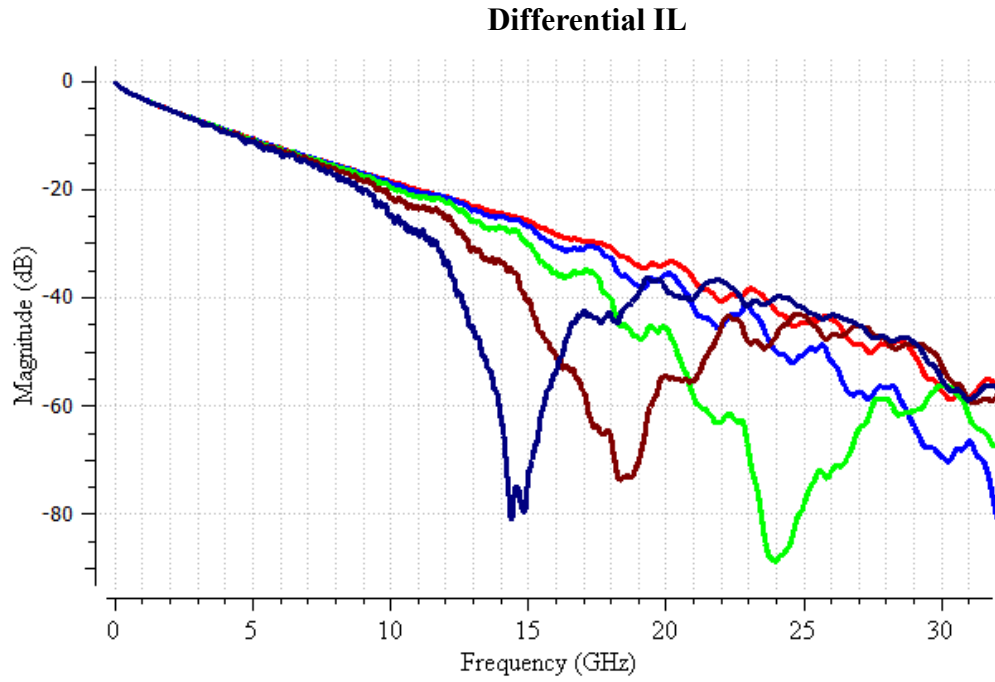
Figure 1.27. The insertion losses of the files with via stub
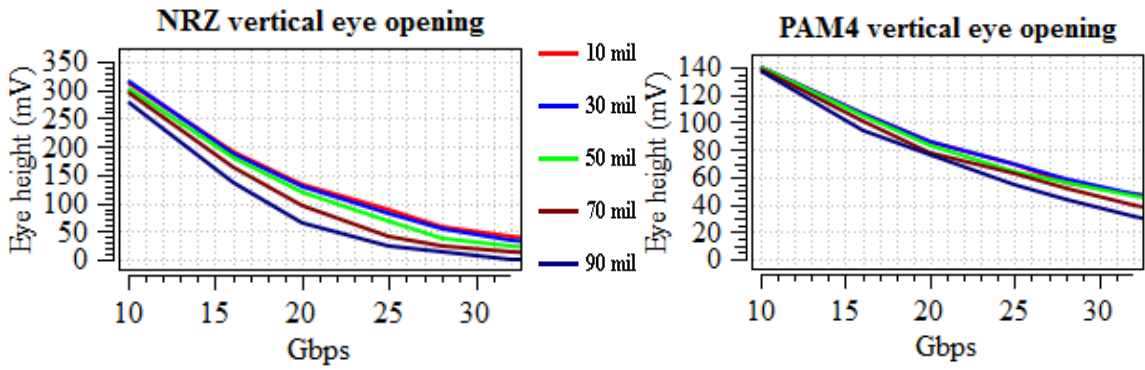
Figure 1.28. The eye openings of the five files for both NRZ and PAM4

Table 1.3. Crucial data rates and dB differences for tests with via stub

	10 mils	30 mils	50 mils	70 mils	90 mils
Data rates (Gbps)	28.6	27	25.5	22.2	19
dB Difference	10.7	11.2	11.7	11.4	11.6

1.5. CONCLUSIONS

Simulation results confirm that PAM4 gives better results with more lossy materials and this advantage increases proportionally to channel loss. PAM4 shows its advantages over NRZ when there are via stubs in the serial link, but it is also affected more by additional reflection loss. Since the crosstalk noise is added to all 4 levels for PAM4, PAM4 is affected more by the crosstalk effect. After adding crosstalk noise, PAM4 eye gets closed more and the crucial data rate tends to start later.

FFE for PAM4 is generally the same as for NRZ, but PAM4 is easier to have overshooting issue and more sensitive to tap values. When DFE is used in combination with FFE, its effectiveness for PAM4 increases, if FFE tap coefficients are chosen in order to avoid overshooting. If maximum optimized FFE coefficients are chosen, DFE loses its effectiveness and the obtained eye height is smaller.

2. CHARACTERISTIC IMPEDANCE EXTRACTION FROM A TRANSMISSION LINE WITH MESHED GROUND PLANES

2.1. INTRODUCTION AND SIMULATION METHODLOGY

Meshed power and ground planes have been widely used in today's flexible PCB designs to satisfy repeatability installation and reliability requirements[18]. And in some industrial process, only the meshed ground planes are allowed due to the manufacturing limitations.

A transmission line referenced to a meshed ground plane is a periodically varying structure, so its cross-section changes along the line. Therefore, its characteristic impedance also changes marginally along the signal propagation direction because the dimension of a single aperture is usually comparable to the trace width [14][15]. So it is reasonable to use effective characteristic impedance to quantify its electrical property.

A typical example of a transmission line with a meshed ground plane is shown in Figure 2.1. The red line is the signal trace and the yellow lines represent the meshed ground planes.
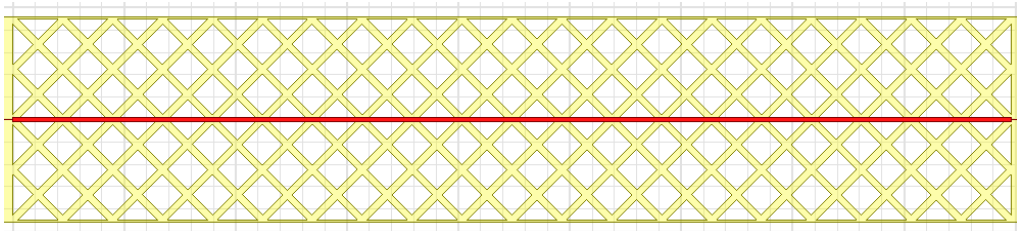
Figure 2.1. Top view of a meshed ground transmission line

In this project, HFSS is used to do full-wave simulation. Figure 2.2 shows the top view of the simulation model. A certain length of transmission line with solid ground line is added to each end of the transmission line with meshed ground plane since a wave port can't be well-defined directly at the end of a meshed ground transmission line. Then a wave

port is defined at the end of the solid ground transmission line. The added transmission lines with solid ground planes are eventually de-embedded to obtain the S-parameters of the transmission lines with meshed ground planes.
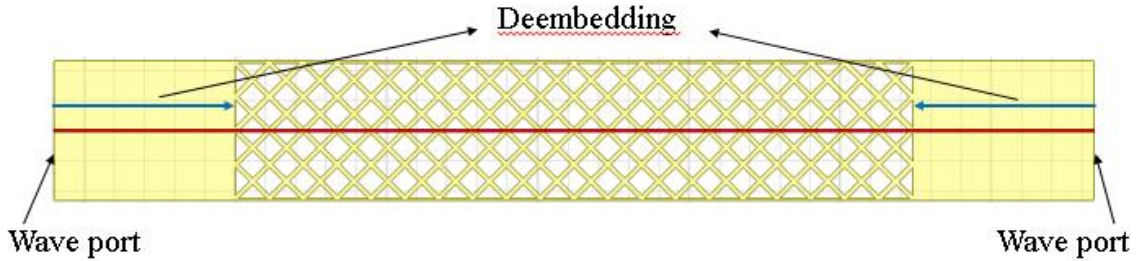
Figure 2.2. Wave port and de-embedding setting

The simulation setups, including the wave port and de-embedding settings, can be validated by cascading the de-embedded results of two lines with the length of L_1 and L_2 and then comparing with the de-embedded results of another line with the length of L_1 + L_2. Figure 2.3 shows the comparison of the results of a 42mm line and the cascaded results of a 28mm line and a 14mm line.
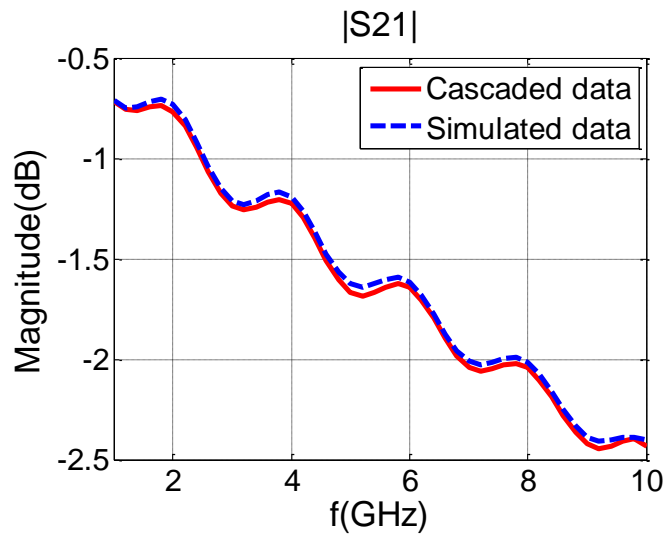
Figure 2.3. The comparison of cascaded S-parameters and directly simulated S-parameters
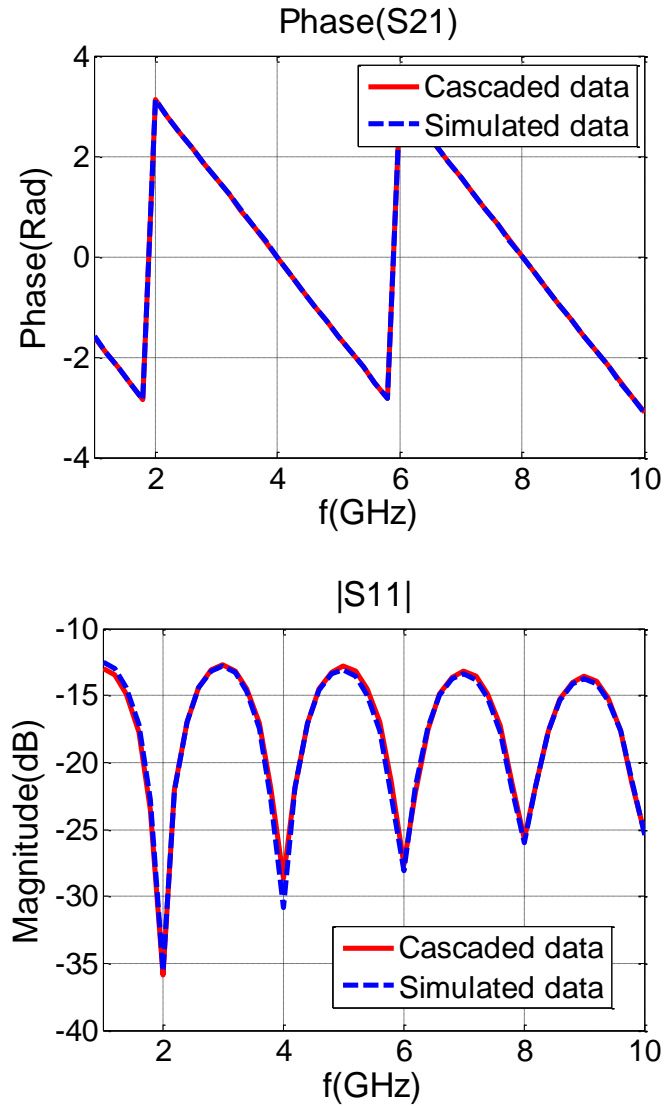
Figure 2.3. The comparison of cascaded S-parameters and directly simulated S-parameters (cont.)

2.2. CHARACTERISTIC IMPEDANCE EXTRACTION FROM FULL-WAVE SIMULATION

The characteristic impedance of a transmission line with meshed ground plane can be extracted from the simulated S-parameters.

2.2.1. Extraction Methodology. First, S-parameters are obtained from full-wave simulations. Then the ABCD matrix of this structure can be determined from S-parameters.

$$
\begin{aligned}
A &= \frac{(1+S_{11})(1-S_{22})+S_{12}S_{21}}{2S_{21}} \\[2mm]
B &= Z_n \frac{(1+S_{11})(1+S_{22})-S_{12}S_{21}}{2S_{21}} \\[2mm]
C &= \frac{1}{Z_n} \frac{(1-S_{11})(1-S_{22})-S_{12}S_{21}}{2S_{21}} \\[2mm]
D &= \frac{(1-S_{11})(1+S_{22})+S_{12}S_{21}}{2S_{21}}
\end{aligned}
\tag{4}
$$

Where Z_n is the port reference impedance.

For a transmission line, its ABCD matrix can be written in terms of its characteristic impedance and propagation constant.

$$
\begin{bmatrix} A & B \\ C & D \end{bmatrix} = \begin{bmatrix} \cosh \gamma l & Z_0 \sinh \gamma l \\ \dfrac{1}{Z_0} \sinh \gamma l & \cosh \gamma l \end{bmatrix}
\tag{5}
$$

Where Z_0, γ and l are the characteristic impedance, propagation constant and length of the line respectively.

So the characteristic impedance and propagation constant of a transmission line can be calculated from its ABCD-parameters.

$$
\begin{aligned}
Z_0 &= \sqrt{\frac{B}{C}} \\[2mm]
\gamma &= \frac{1}{l} \cosh^{-1} A
\end{aligned}
\tag{6}
$$

However, the magnitude of Z_0 obtained from this equation usually jumps up and down near some frequencies. This is because the C-parameter is a hyperbolic sine function, its magnitude has peak points and zero points as shown in Figure 2.4. Near the zero points

the magnitude of C-parameter is very small so it is extremely sensitive to noise or numerical error. The peak points are less sensitive hence it is reasonable to use these points to improve the results.
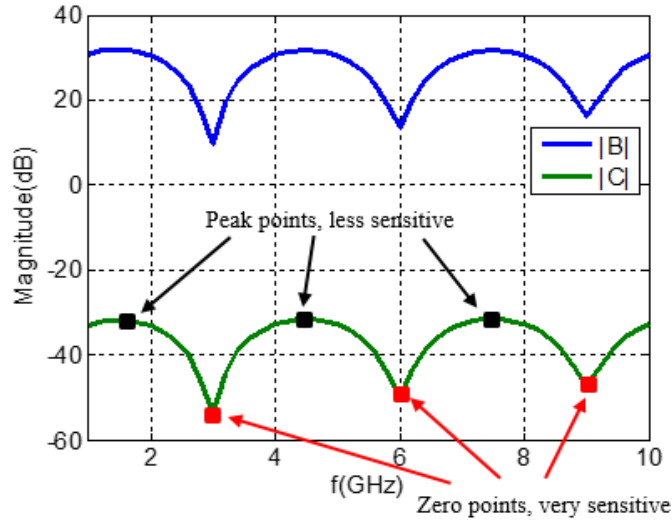
Figure 2.4. Peak points and zero points in C-parameter

The fitting algorithm is based on W-Element transmission line model to obtain the per-unit-length RLGC parameters. The W-Element transmission line equation is:

$$\frac{dV}{dx} = -[R_0 + R_f \sqrt{f}(1+j) + j2\pi f L_{pul}]I$$
$$\frac{dI}{dx} = -[G_0 + G_f f + j2\pi f C_{pul}]V \tag{7}$$

Where R_0, R_f, G_0, G_f are all frequency independent parameters. The per-unit-length impedance and admittance of the line are:

$$Z = R_0 + R_f \sqrt{f}(1+j) + j2\pi f L_{pul}$$
$$Y = G_0 + G_f f + j2\pi f C_{pul} \tag{8}$$

If the peak points in the C-parameter satisfy this equation, two sets of equations can be constructed. As they are complex equations, the real part of them are taken first.

$$\begin{bmatrix} 1 & \sqrt{f_1} \\ \vdots & \vdots \\ 1 & \sqrt{f_n} \end{bmatrix} \begin{bmatrix} R_0 \\ R_f \end{bmatrix} = \begin{bmatrix} Real(Z_1) \\ \vdots \\ Real(Z_n) \end{bmatrix}$$
$$\begin{bmatrix} 1 & f_1 \\ \vdots & \vdots \\ 1 & f_n \end{bmatrix} \begin{bmatrix} G_0 \\ G_f \end{bmatrix} = \begin{bmatrix} Real(Y_1) \\ \vdots \\ Real(Y_n) \end{bmatrix}$$

(9)

Where f_n are the frequencies of the peak points in the C-parameter, and Z_n, Y_n are the corresponding per-unit-length impedance and admittance values at these frequencies. From equation (6), the characteristic impedance and propagation constant can be obtained from ABCD-parameters. According to equation (10), the per-unit-length impedance and admittance can also be obtained from ABCD-parameters as shown in equation (11).

$$Z = Z_0 \times \gamma$$
$$Y = \gamma / Z_0$$

(10)

$$Z_n = \frac{1}{l} \sqrt{\frac{B_n}{C_n}} \times \cosh^{-1} A_n$$

$$Y_n = \frac{1}{l} \sqrt{\frac{C_n}{B_n}} \times \cosh^{-1} A_n$$

(11)

Where An, Bn and Cn are A-parameter, B-parameter and C-parameter at these frequencies respectively, l is the length of the transmission line.

The next step is to solve equation (9) for the least-square solution with constraints that R_0, R_f, G_0, G_f are all non-negative values.

From the imaginary part of equation (8), the per-unit-length L and C can be calculated by equation (12).

$$2\pi f_n L_{n,pul} + R_f \sqrt{f_n} = imag(Z_n)$$
$$2\pi f_n C_{n,pul} = imag(Y_n)$$

(12)

There are *n* solutions for these two sets of equations. The average value is taken as the estimated per-unit-length inductance and capacitance of the transmission line.

From the RLGC parameters obtained at the previous steps, the characteristic impedance can be calculated as:

$$Z_{0,extracted} = \sqrt{\frac{R_0 + R_f \sqrt{f}(1+j) + j2\pi fL_{pul}}{G_0 + G_f f + j2\pi fC_{pul}}}$$ (13)

2.2.2. Validation with Full-Wave Simulation. To validate this effective characteristic impedance extraction methodology, a test model is built as shown in Figure 2.5. A trace is referenced to a meshed ground plane. The distance between the trace and the meshed reference plane, h1, is 8μm. The thickness of the trace, t, is 6μm and the distance between the trace and the solid plane, h2, is set to 37μm. Although there is another complete plane above the trace, the trace is much closer to the meshed plane so its electrical properties is still dominated by the meshed ground plane. The geometric parameters of this example are described as follows. The diagonal pattern dimension, a, is 1.4mm; hole to hole distance, b, is 70μm. The dielectric constant of the material is 3.2 and the loss tangent is 0.035.
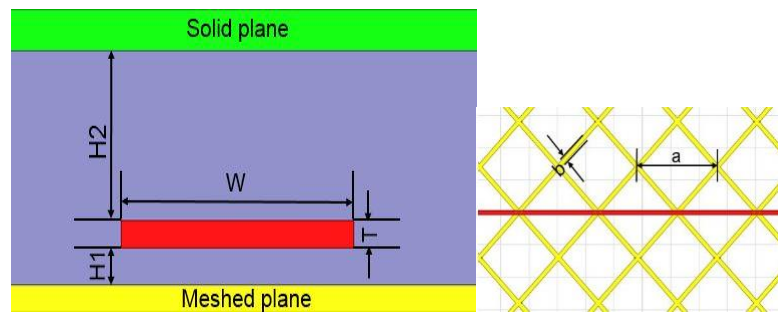

Figure 2.5. Geometry of the example

When trace width is 70μm, the extracted effective characteristic impedance at 5GHz is 45.67Ω. The magnitude of the effective characteristic impedance in frequency

domain is plotted in Figure 2.6. The impedance value increases when the frequency gets lower and gradually gets converged at high frequencies, which follows the physics. The corresponding effective per-unit-length RLGC parameters are: L_{pul} = 288.58nH/m, C_{pul} = 139.9pF/m, R_0 = 11Ω/m, G_0 = 0S/m, R_f =0.0014 Ω/m-sqrt(Hz) and G_f = 2.25e-11S/m-Hz. In order to verify this equivalent transmission model, S-parameters for this 21mm trace is recalculated from the extracted per-unit-length RLGC parameters and compare with full-wave simulations. Figure 2.7 shows the comparison of the S-parameter obtained by full-wave simulations and the above methodology. Figure 2.8 shows the comparison of the propagation constant obtained by full-wave simulations and this methodology. The results obtained from this methodology and full-wave simulations have a good agreement in both the magnitude and the phase of the insertion loss. Though there is some discrepancy in return loss, the levels are quite close. The extracted propagation constant also agrees with the simulation data, which further validates this approach.

Figure 2.6. The effective characteristic impedance

(a)

(b)

(c)

Figure 2.7. Comparison of S-parameters, (a) magnitude of insertion loss, (b) phase of insertion loss, (c) magnitude of return loss
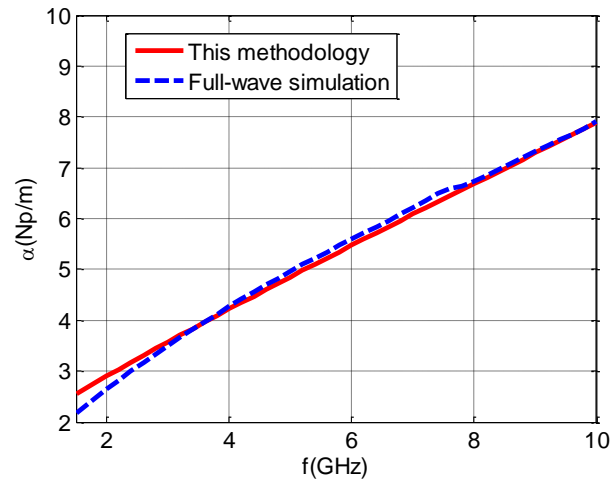
(a)
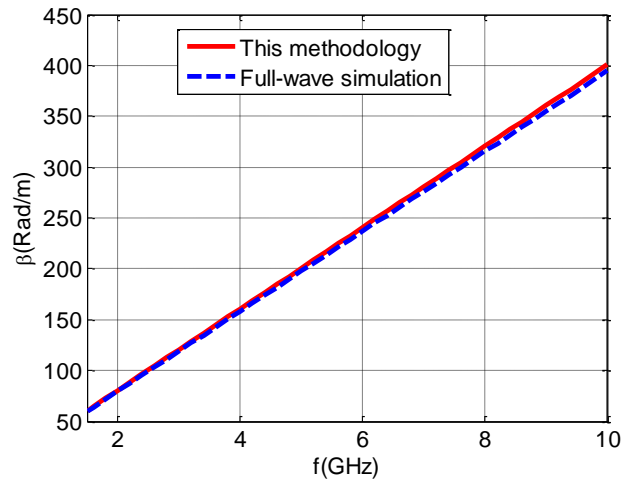
(b)

Figure 2.8. Comparison of propagation constant, (a) real part of γ (b) imaginary part of γ

Another test case is a stripline with two meshed reference layers as shown in Figure 2.9. The distance between the trace and the lower meshed reference plane, *h1*, is 20μm. The thickness of the trace, *t*, is 10μm and the distance between the trace and the upper meshed layer, *h2*, is set to 60μm. The trace width, *w*, is 60μm. The geometric parameters of this example are described as follows. The diagonal pattern dimension, *a*, is 0.7mm; hole to hole distance, *b*, is 200μm.

For this test case, the corresponding effective per-unit-length RLGC parameters are: $L_{pul} = 346.83$nH/m, $C_{pul} = 122.1$pF/m, $R_0 = 95.4\Omega$/m, $G_0 = 0$S/m, $R_f = 0.0017\ \Omega$/m-sqrt(Hz) and $G_f = 1.39$e-11S/m-Hz. The magnitude of the effective characteristic impedance in frequency domain is plotted in Figure 2.10. And the comparison with full-wave simulation is shown in Figure 2.11. The results also agree with each other though there is some deviation in S11. The discrepancy mainly comes from the approximations in the algorithm. In these two cases, it can be shown that the extracted R term is not that stable, though the impedance value is OK as it is mainly determined by the L term and C term.

Figure 2.9. Geometry of the second example
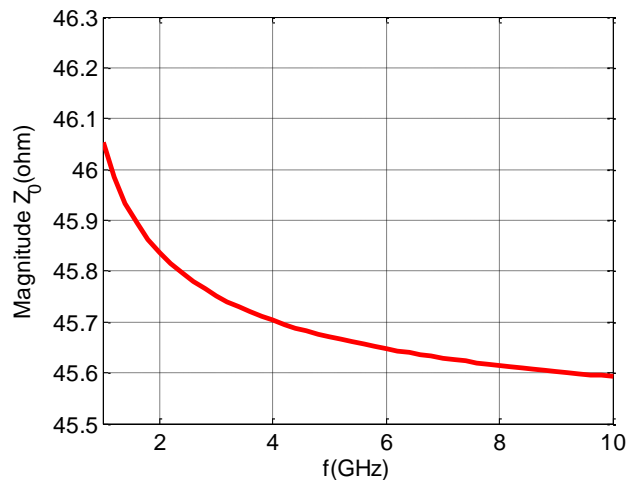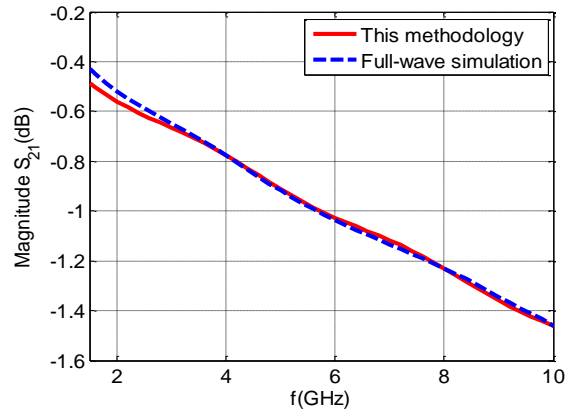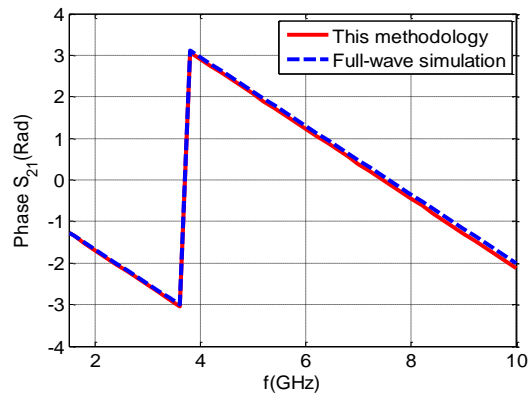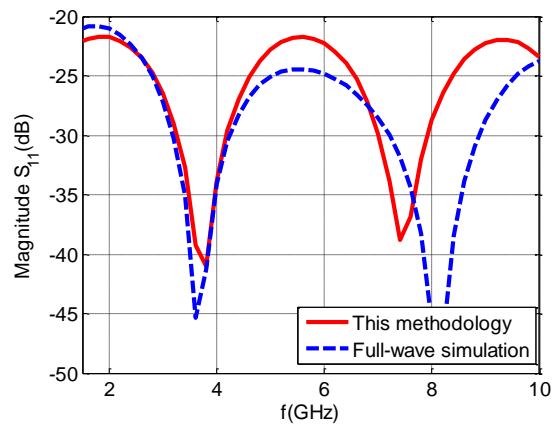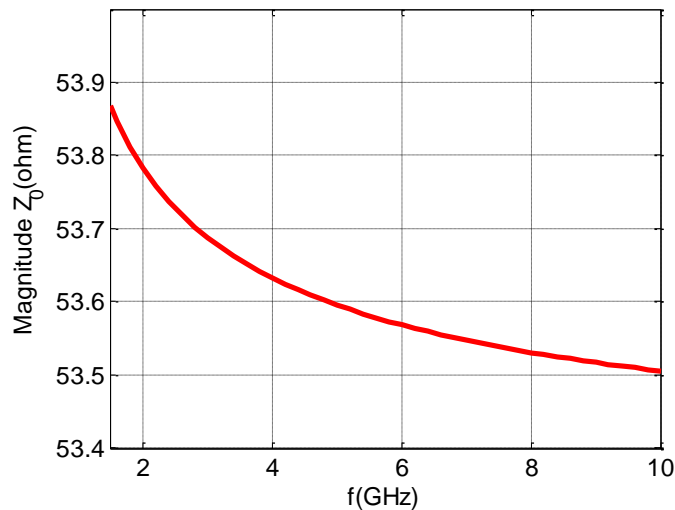

Figure 2.10. The effective characteristic impedance
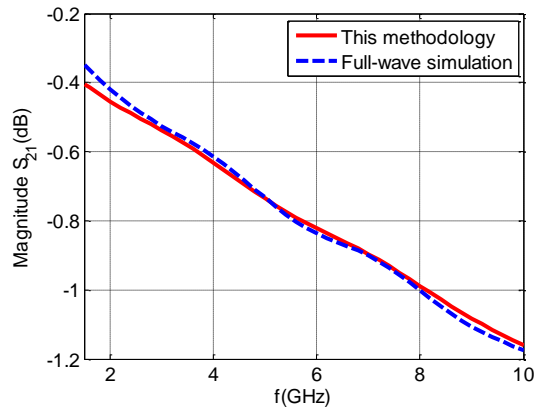
(a)
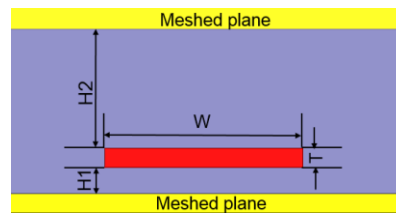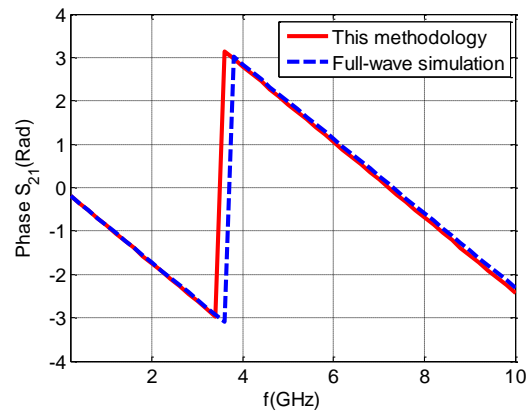

(b)
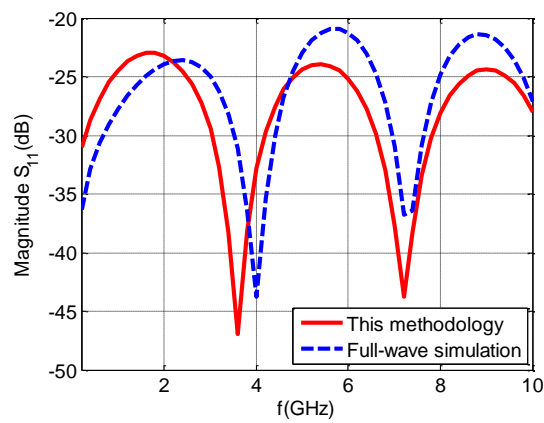
(c)

Figure 2.11. Comparison of S-parameters, (a) magnitude of insertion loss, (b) phase of insertion loss, (c) magnitude of return loss

To further validate this extraction methodology, the geometric impact of trace width and mesh size is investigated. The extracted per-unit-length inductance and capacitance of the first test case are also listed for comparison.

The trace width is increased from 30μm to 90μm gradually and the effective characteristic impedance of each case is extracted by the algorithm described previously. Table 2.1 summarizes the extracted per-unit-length inductance and capacitance values. The per-unit-length inductance decreases and per-unit-length capacitance increases as trace becomes wider, which follows the physics. As a result, the effective characteristic impedance decreases when trace width becomes larger.

Table 2.1. Per-unit-length inductance and capacitance for different trace width

Width(μm)	PUL Inductance(nH/m)	PUL Capacitance(pF/m)
30	426	86.1
40	378	98.0
50	345	110
60	314	123
70	293	135
80	277	147
90	254	160

The effect of aperture dimension is also investigated. The diagonal distance of the mesh pattern, a, increases from 1.6mm to 2.0mm while other parameters are fixed. Less solid reference conductor is put beneath the trace as a increases. Consequently per-unit-length capacitance becomes smaller as shown in Table 2.2. In this example, as b is only 70μm, much smaller than a, so the variation of per-unit-length capacitance is not large when a increases from 1.6mm to 2mm.

Table 2.2. Per-unit-length inductance and capacitance for different a

W=90μm	PUL Inductance(nH/m)	PUL Capacitance(pF/m)
1.6mm	254	160
2.0mm	254	153
W=60μm	PUL Inductance(nH/m)	PUL Capacitance(pF/m)
1.6mm	314	123
2.0mm	315	118

2.3. IMPEDANCE ESTIMATION USING DOE METHOD

To quickly estimate the characteristic impedance of a meshed ground transmission line when the given geometry is in a certain range, the DoE method is used. Since there are many variables in a meshed ground transmission line, it is not practical to take all of them into DoE. A new variable called "meshed ground factor" is introduced. The meshed ground factor is defined as the ratio of the characteristic impedance of the meshed ground transmission line to the solid ground transmission line. This factor is the goal of the experimental designs. It is obvious that the meshed ground factor is a function of mesh pattern parameters and also a function of stack-up geometry.

The expressions of the meshed ground factor for a certain stack-up in terms of the mesh pattern parameters are first obtained from DoE. Then the expressions combined with related stack-up parameters are calculated by linear interpolation. Finally the estimated characteristic impedance is calculated by multiplying the characteristic impedance of the solid ground impedance with the same geometry and the meshed ground factor.

2.3.1. Microstrip Line. The stack-up of a microstrip line with meshed ground plane is shown in Figure 2.12. It is assumed that the meshed ground factor is mainly a function of w/h_1 and independent of the dielectric constant.
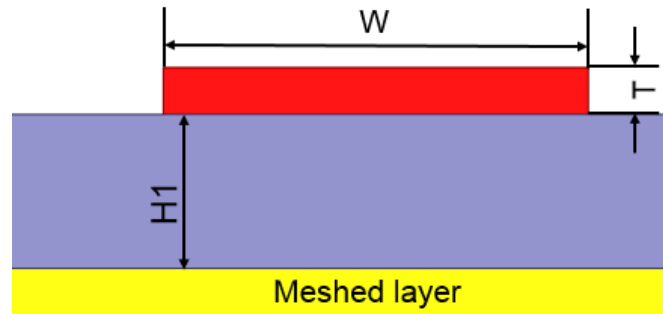
Figure 2.12. The stack-up of a microstrip line with meshed ground plane

For a certain w/h_1 value, full-factorial design method is used to derive the meshed ground factor's expression in terms of the mesh pattern parameters, the a and b value in Figure 2.13. Then when the w/h_1 value is in the range, the final expression of the meshed ground factor is calculated by linear interpolation. Finally, the meshed ground factor from the last step is multiplied with the impedance of the solid ground transmission line from the analytical formula to obtain the impedance of a meshed ground transmission line. The flow of the calculation is shown in Figure 2.14.
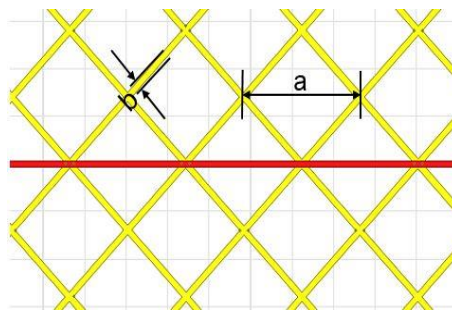
Figure 2.13. Two mesh pattern parameters
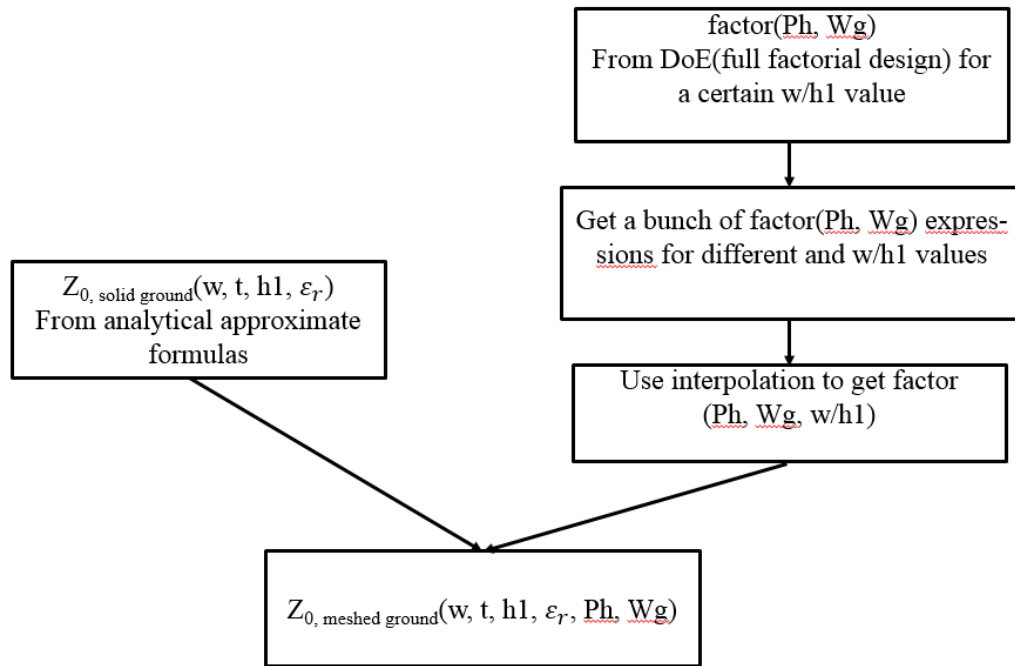
Figure 2.14. The flow of the calculation method for microstrip

The analytical formula of the solid ground microstrip line is[17]:

$$Z_{0,\text{solidground}} = \frac{120\pi}{\sqrt{\varepsilon_{r,\text{eff}}}} \left(\frac{1}{\frac{w'}{h_1} + 1.393 + 0.667 \ln(\frac{w'}{h_1} + 1.444)} \right)$$

Where $\varepsilon_{r,\text{eff}} = \frac{\varepsilon_r + 1}{2} + \frac{\varepsilon_r - 1}{2} \sqrt{\frac{w}{(w + 12h_1)}}$ $\quad (\frac{w}{h_1} > 1)$, $\hfill (14)$

$$w' = w + \frac{t}{2\pi}(4 - \frac{1}{2}\ln((\frac{t}{h})^2 + (\frac{1}{\pi(\frac{w}{t} + 1.1)})^2))(\frac{1 + \frac{1}{\varepsilon_r}}{2})$$

The range for the mesh size parameter is 150μm ~800μm and the range for the ground width parameter is 30μm ~200μm. In the full-factorial design, 6 sample points are chosen for the mesh size and 4 sample points are chosen for ground width parameter. There are 24 experiments in one design.

The estimated w/h_1 value is between 4 and 7, the samples points are 4, 5, 6, 7. So there are 4 expressions from 4 full-factorial designs.

To test this prediction method, some cases with random geometries are picked and simulated in full-wave simulators, then the results from full-wave simulations are compared with the predicted results in Table 2.3. For these cases, the differences between the prediction and the full-wave simulation are within 5%.

Table 2.3. The comparison results for microstrip line

	Full-wave	Prediction	Relative error
Case1 a=400μm, b=200μm	58.0064Ω	58.67Ω	1.15%
Case2 a=500μm, b=155μm	60.8226Ω	63.3Ω	4.1%
Case3 a=600μm, b=80μm	72.5327Ω	74.79Ω	3.1%
Case4 a=400μm, b=160μm	63.9217Ω	66.26Ω	3.66%
Case5 a=360μm, b=200μm	52.5013Ω	54.75Ω	4.3%
Case6 a=420μm, b=150μm	58.1671Ω	60.44Ω	3.9%

2.3.2. Strip Line. The stack-up of a strip line with meshed ground plane is shown in Figure 2.15. It is assumed that the meshed ground factor is mainly a function of w/h_1 and h_2/h_1 independent of the dielectric constant.
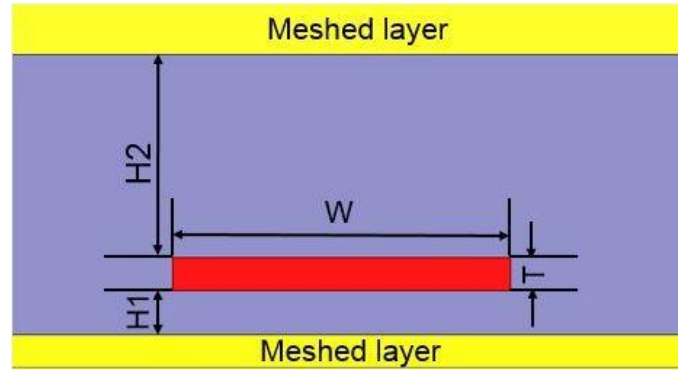
Figure 2.15. The stack-up of a strip line with meshed ground plane

Similarly, for a certain w/h_1 and h_2/h_1 value, full-factorial design method is used to derive the meshed ground factor's expression in terms of the mesh pattern parameters, the a and b value in Figure 2.13. Then when the w/h_1 value is in the range, the final expression of the meshed ground factor is calculated by linear interpolation.

The analytical formula of the solid ground strip line is[17]:

$$Z_{0,\text{solidground}} = \frac{\eta_0}{\sqrt{\varepsilon_r}}\left(\frac{1}{\dfrac{w/b}{\gamma}+\dfrac{w/b}{\beta-\gamma}+2C_f}\right) \tag{15}$$

Where
$$C_f = \frac{1}{\pi}\left(2\ln\frac{1}{\gamma(\beta-\gamma)}+\frac{1}{\gamma(\beta-\gamma)}(F(\frac{t}{2b})-F(\frac{cl}{b}))\right)$$

$$F(x) = (1-2x)((1-x)\ln(1-x)-x\ln x)$$

$$\gamma = \frac{cl}{b}-\frac{t}{2b}, \beta = 1-\frac{t}{b}, cl = \frac{b-s}{2}$$

Where b, s, t are shown in Figure 2.16
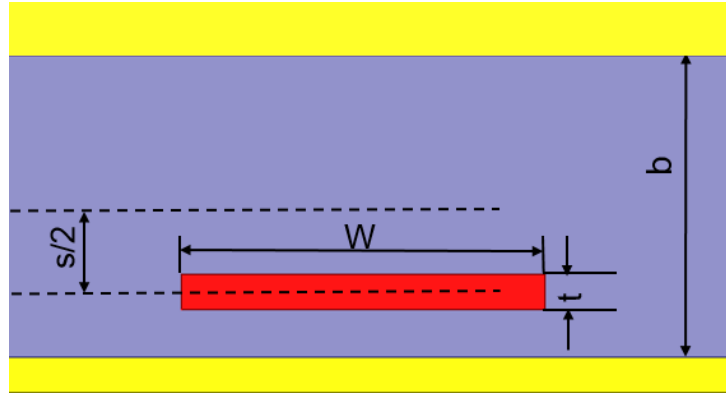
Figure 2.16. Illustration of the variables used in the analytical formula

The comparison results are in Table 2.4.

Table 2.4. The comparison results for strip line

	Full-wave	Prediction	Relative error
Case1 a=290μm, b=150μm	55.3137Ω	56.1575Ω	1.53%
Case2 a=400μm, b=150μm	62.3139Ω	61.0509Ω	2%
Case3 a=300μm, b=200μm	51.748Ω	50.693Ω	2%

2.4. CONCLUSIONS

Effective characteristic impedance of a transmission line referenced to a meshed ground plane is extracted from an equivalent transmission line model based fitting methodology. The validity of this methodology has been confirmed with the results from full-wave simulations. The extracted per-unit-length inductance and capacitance also follow the physical trend when geometry changes. The drawback of this method is that it assumes the full-wave simulation results at some frequency points are correct and accurate,

which may not always be true. As the data at these frequency points are used in fitting, the accuracy of the extracted results may be compromised if the assumption is not satisfied.

To predict the characteristic impedance without running a full-wave simulation when the geometry is in a given range, the above fitting method is combined with DoE method. By doing full-factorial design and interpolation, the meshed ground factor is obtained. Finally the factor is multiplied with the characteristic impedance of solid ground transmission lines from analytical formulas to get the predicted characteristic impedance of meshed ground transmission line.

BIBLIOGRAPHY

[1]   M. Brown, M. Dudek, A. Healey, L. B. Artsi, R. Mellitz, Ch. Moore, A. Ran, P. Zivny, "The state of IEEE 802.3bj 100 Gb/s Backplane Ethernet", DesignCon 2014.

[2]   IEEE P802.3bj™ 100 Gbps Backplane and Copper Cable Task Force materials, http://www.ieee802.org/3/bj.

[3]   IEEE 802.3 400 Gbps Ethernet (400 GbE) Study Group materials, http://www.ieee802.org/3/bs/.

[4]   A. Sheikholeslami, "Multi-Level Signaling for Chip-to-Chip and Backplane Communication", 39th International Symposium on Multiple-Valued Logic, 2009.

[5]   A. Healey, Ch. Morgan, M. Shanbhag, "Beyond 25 Gbps: A Study of NRZ & Multi-Level Modulation in Alternative Backplane Architectures", DesignCon 2013.

[6]   D. Correia, V. Shah, Ch. Chua, P. Amleshi, "Performance Comparison of Different Encoding Schemes in Backplane Channel at 25Gbps+", DesignCon 2013.

[7]   A. Healey, C. Morgan, "A Comparison of 25 Gbps NRZ & PAM-4 Modulation Used in Legacy & Premium Backplane Channels", DesignCon, 2012.

[8]   H. Badaoui, Y. Frignac, P. Ramantanis, B. E. Benkelfat, M. Feham, "PRQS Sequences Characteristics Analysis by Auto-correlation Function and Statistical Properties", International Journal of Computer Science Issues, Volume 7, Issue 4, No 4, pp 39-43, July, 2010.

[9]   J. Lee, M.-Sh. Chen, H.-D. Wang, "Design and Comparison of Three 20-Gb/s Backplane Transceivers for Duobinary, PAM4, and NRZ Data", IEEE Journal of Solid-State Circiuts, Vol. 43, No. 9, 2008.

[10]   H. Zhang, B. Jiao, Y. Liao, G. Zhang, PAM4 Signaling for 56G Serial Link Applications, DesignCon2016.

[11]   Fei Yuan, Adaptive Decision Feedback Equalizations for Multi-Gbps Serial Links, Sensor Netw Data Comm., 2015.

[12]   H. Zhang, F. Rao, K. Dong, G. Zhang, "IBIS-AMI Modeling and Simulation of 56G PAM4 Link Systems", DesignCon 2015.

[13]   N. Dikhaminjia, J. He, M. Tsiklauri, J. Drewniak, A. Chada, M. Zvonkin, B. Mutnury, E. Hernandez, "High-Speed Serial Link Challenges using Multi-Level Signaling", EPEPS 2015.

[14]   S. Wu, H. Shi, M. Herndon, B. Cornelius, M. Halligan, and J. Fan, "Modelling and analysis of a trace referenced to a meshed ground plane," 2011 IEEE EMC symposium, pp. 137-141, 2011.

[15]   J. Kim, T. Lee, D. Kim, J. Lee, S. Lee, H. Kim, J. Park, and C.Cheon, "Analysis of Coupling Characteristics between Transmission Lines with a Buried Meshed-Ground in LTCC-MCMs," 2002 IEEE MTT-S Syposium Digest, vol. 2, pp.825-828, 2002.

[16]   H. Lee and J. Kim, "Electrical Characteristics of Single and Coupled Stripline on Meshed Ground Plane in High-speed Package," Electronic Materials and Packaging, pp261-267, 2001.

[17]   B. Wadell, "Transmission Line Design Handbook", 1991.

[18]   Y. Li, E. Bradawy, E. Sharawy, L. Polka, A. Madrid, J. Liao, D. Figueroa, "Modelling and Experimental Validation of Interconnects with Meshed Power Planes," Proceedings of Electronic Components and Technology Conference, pp. 1158-1162, 1997.

VITA

Jiayi He was born in Wuhan, Hubei, China. He received his B.S. degree in Electronics and Information Engineering from Huazhong University of Science and Technology, Wuhan, China, in 2014. He joined the EMC Laboratory in the Missouri University of Science and Technology, Rolla, in 2014 and received the M.S. degree of Electrical Engineering in May 2017. He worked as a Co-op Engineer at DELL SI Team in 2016.